MEASUREMENTS OF SPIN TORQUES DUE TO REORIENTABLE ANOMALOUS HALL SPIN CURRENTS

A Dissertation

Presented to the Faculty of the Graduate School

of Cornell University

In Partial Fulfillment of the Requirements for the Degree of

Doctor of Philosophy

by

Jonathan Gibbons

August 2018

MEASUREMENTS OF SPIN TORQUES DUE TO REORIENTABLE ANOMALOUS HALL SPIN CURRENTS

Jonathan Gibbons, Ph. D.

Cornell University 2018

This dissertation discusses spin currents generated by the anomalous Hall effect in ferromagnetic materials. It primarily presents second harmonic Hall technique measurements with an in-plane magnetic sensor layer that demonstrate that the spin polarization of such spin currents orients itself parallel to the magnetization of the generating layer. Hence the work demonstrates that one can control the spin polarization of spin currents generated in this way, such that torques may be actively reoriented during measurement by controlling the magnetization of the generating layer. By these measurements, this work also estimates the spin torque efficiency of the alloy of iron and gadolinium used for this measurement to be about 1%. This dissertation then discusses ongoing measurements using the spin torque ferromagnetic resonance technique modified by application of a DC bias current to characterize the size of the anomalous Hall spin torque efficiency in a cobalt holmium alloy and several other materials. The author presents related ongoing efforts with additional experimental techniques to understand and utilize the anomalous Hall spin current effectively. This work also discusses practical applications for reorientable spin torques.

BIOGRAPHICAL SKETCH

Jonathan Daniel Gibbons was born June 7, 1990 in Renton, Washington, to Laurence Gibbons and Deborah Gibbons, the fourth and last of their children, with three older brothers, Christopher, Michael, and Timothy. After two years in Washington, his family moved to Pittsburgh, Pennsylvania, so that his mother could pursue a doctorate in organizational behavior from Carnegie Mellon University. His father, who finished his education with a Bachelor's degree in Mathematics from University of Washington, found work at a Remote Encoding Center. Five years later, Jonathan moved with his mother, Timothy, and Michael to Atlanta, Georgia, where his mother became a professor at Georgia State University. His family moved quite a lot and often took full summers off to go on long road trips through the USA and Canada. In 2003, they traveled as far as Alaska, and even camped on the Arctic circle. Eventually, they settled for four years in metro Atlanta while Michael studied Physics at Georgia Tech University nearby.

As a child, Jonathan was intelligent, curious, and diligent, and generally connected better with his instructors than with other students. Consequently, he frequently spent his free time at school programming simulations, half-baked video games, and other odds and ends on his TI-83 Plus calculator, which had only recently been released. Jonathan excelled in most subjects save handwriting, but he particularly performed well in math and science, and Michael happily gave him

early exposure to physics problems and the intellectual quandaries they raised.

In 2004, his family moved to Monterey, California, while Michael remained at Georgia Tech to pursue a PhD in atomic physics, and Jonathan began high school in the Monterey Academy of Oceanographic Sciences at Monterey High School. While there, Jonathan exhausted all of the mathematics courses available at his school and enrolled concurrently at the community college to take more advanced statistics and calculus courses. During this time, he also joined the school's drama program, which helped him overcome his social ineptitude. He interned with Ajay Mehra, a professor at the University of Kentucky, writing MATLAB modeling code.

Jonathan graduated from Monterey High School as Valedictorian and received scholarships from the Monterey Rotary Club, the Church of the Wayfarer Methodist Church, and the Fellowship of Christian Athletes that paid for much of his tuition to UC Berkeley, where he did his undergraduate studies. Immediately determined to study Physics, he enrolled in honors Physics courses, and, after a bit of a rocky start, succeeded academically throughout his major. In his junior year, he took a course on solid state Physics, and found himself intrigued by the spatial reasoning required to solve problems in the field, and elected to pursue related research. He joined Prof. Zi Qiang Qiu's research group, using MOKE and XMCD at the nearby Advanced Light Source (ALS) to probe the magnetization of sputtered materials.

Jonathan graduated from Berkeley with high honors, and was accepted to PhD programs in physics at several universities, including Cornell University,

where David MacNeill and Jennifer Grab helped show him around. He loved his visit and the school's approach to research enough that he decided to attend Cornell. After half a year of studies, he decided that he wanted to join the Ralph group because of its intriguing research topics and the excellent mentoring that Professor Ralph provides, a decision he has not regretted. In addition to participating on exciting research projects with Prof. Ralph, Jonathan has enjoyed the opportunity to collaborate with Chang-Beom Eom's group at the University of Wisconsin Madison researching spin torque in novel material structures. In future, Jonathan hopes to apply his expertise in physics to groundbreaking research and practical problems.

ACKNOWLEDGMENTS

My time at Cornell University has been fulfilling and enjoyable due primarily to the support of the wonderful individuals I have had the opportunity to work with and alongside. Most of all, I wish to thank Prof. Dan Ralph, my thesis advisor, for being continuously supportive and providing insightful and wise advice regarding everything from experimental concerns to academic writing, and even such issues as work-life balance. I remember that when I first joined the Ralph group, he assured me (not in precisely these words) that he did his best to give his graduate students an environment where they could thrive, and he was true to his word. Dan is a genuine mentor to his students, and considers their best interests in his decision-making, for which I am truly grateful. In addition, his commitment to a high level of academic principles and love of interesting physics have both shaped the way I view the academic world and physics in general. Beyond being an exemplary researcher, Dan Ralph is also a phenomenal advisor and mentor, and I am very glad to have had the opportunity to study under him.

I have received substantial support from the members of the Ralph and Buhrman groups, and would particularly like to thank my colleague and mentor within the Ralph Group, Alex Mellnik, for training me with both fabrication and the proper methods of experimentation, and Peter Mintun, his undergraduate student, who often helped with processes when Alex was absent or busy. Both of these individuals showed patience in working with me, and never got irritated with any of

my mistakes. I would also like to thank Jennifer Grab and David MacNeill, who worked alongside me for a span of years, for providing a great deal of support and advice during my work at Cornell University, throughout our friendship and coworker relationships. David MacNeill has been a great coauthor, patiently suggesting exactly how I might re-write the entire paper before it would be acceptable. I would also like to thank Neal Reynolds, who has walked the path of the graduate student alongside me from my very first year, and whose advice and aid has been indispensable to me during my time in the Ralph group, and Colin Jermain, whose friendly manner and willingness to help and offer advice whenever necessary, as well as to include me in some of his own research, helped me during my early time in the research group. I would also like to thank Greg Stiehl for taking an active interest in my research and providing me with helpful critiques and insightful advice at various points in my work. Finally, thanks to all of the Ralph and Buhrman group members, including Ruofan Li, Vishakha Gupta, Marcos Guimaraes, Luis Henrique Vilela Leão, John Heron, Sriharsha Aradhya, Graham Rowlands, Praveen Gowtham, Chi-Feng Pai, Alison Rugar, Yongxi Ou, Minh-Hai Nguyen, and Ryan Tapping for their help and camaraderie during my time at Cornell.

Thanks to Nate Ellis for encouraging me and helping me with machine shop troubles, and for training me to use the equipment. I have also greatly appreciated the shared resources at the Center for Materials Research, and the people who oversee those shared resources, especially Steve Kriske, who has helped me fix

many a broken wire bonder. Thanks also to all of the staff of the Cornell NanoScale Science and Technology Facility, and especially Garry Bordonaro for his help with photolithography processes and equipment, and Beth Rhoades for her help with various equipment around the CNF, particularly photolithography equipment and the Class 2 resist room equipment, and for being supportive and helpful every time I've encountered her.

I would like to thank my collaborators in Wisconsin, Prof. Chang-Beom Eom, his postdoc, Tianxiang Nan, and graduate student, Trevor Anderson. Working with their research group has been a pleasure, and the results have been both intriguing and productive. Their research group made me welcome, and I appreciate their invitation to work with them on their excellent research projects.

Thanks to Prof. Robert Buhrman for his advice and help with my research, particularly on our collaborative paper, as well as for serving on my advisory committee. I also thank Prof. Eun-Ah Kim for providing advice and serving on my committee, and Prof. Erich Mueller, for agreeing on short notice to fill in on my committee, as Prof. Kim will be absent for my thesis defense.

Finally, I must take some time to thank those whose efforts enabled me to come to where I am today. Without continuous support from family, friends, and mentors throughout my youth, I would likely never have arrived in the physics doctoral program at Cornell University.

I would like to acknowledge the encouragement I received from all of my teachers and advisors, especially my instructors in the sciences. Thank you to

Prof. Zi Qiang Qiu, with whom I did research as an undergraduate, for continuously encouraging me to ask interesting questions about the world around me. His insights into life and nature, and simple style of explanation, helped me to understand the concepts of experimental condensed matter physics. It was also by his recommendation that I applied to Cornell University, which ultimately proved to be a wonderful graduate school. Additionally, I would like to thank Ali Tan and Jia Li, who provided mentorship to me and allowed me to work with them on their experiments during my time as an undergraduate at UC Berkeley. It was through these two that I first heard about the research of Prof. Ralph's group at Cornell.

From a young age, I have been fortunate to receive academic guidance from my family, who encouraged me to pursue my interests in the hard sciences. From helping out with last minute projects to answering questions about the physical world, and, later in my life, providing me with opportunities and projects to deepen my understanding of numerical representations of real-world phenomena, they have always been supportive of my intellectual pursuits. All of my older brothers, Timothy, Christopher, and Michael, attended graduate school, and established expectations for me and encouraged me on my journey, and my grandparents provided unerring support and belief in my abilities that helped me to aspire to higher goals. It is thus largely through my family's help that I have prospered in my studies, and their continued support proves invaluable to me even now. In this regard, I feel the need to particularly acknowledge the contributions of my second-eldest brother, Michael Gibbons, who himself has a doctorate in

physics. He encouraged me in my pursuit of the field, and often aided me when I failed to understand one of my topics of study. A warm thank you to my mother, Deborah Gibbons, who works as a professor in Organizational Behavior, and who, in addition to providing unrelenting support for my efforts in higher education, also included me in many projects related to numerical modeling and simulation that gave me a sense for the nature of research.

In addition to providing me with academic support, my family helped develop in me a strong code of ethics and sense of responsibility that has helped me beat the stresses and concerns of graduate school, and they have helped to uphold my faith in God. The faith that they helped to cement has strengthened my sense of purpose and deepened my sense of wonder regarding the natural world and its laws, and has driven me to seek deeper understanding of the world around me. It is safe to say, I think, that without my faith which they nurtured, I would not love physics as I do.

TABLE OF CONTENTS

CHAPTER 1

SPIN TORQUES AND NONVOLATILE MEMORY

1.1 MRAM and Nonvolatile Memory

Scientists and engineers have pursued efficient memory storage since the advent of computing, because high-density information storage is necessary for complex computing applications. As processors have improved and processing times have decreased, difficult calculations have become much easier, and, with this ease, more available to the layperson. With more complex calculations, more and more memory becomes necessary, and denser, more efficient systems of memory storage become desirable. With increasing demand, reproducibility and standardized production processes gain importance. Early memory could be achieved through punch cards, but the quantity of data now exceeds anything that could be stored in such an archaic medium, and the inconvenience of punch cards renders them inaccessible to the public. Dense, effective information storage requires a system tailored to the problem. A variety of solutions have been formulated, but none of them are quite ideal, and, as computing evolves, will need to be continuously improved. Historically, memory density has increased through decreasing bit sizes, but there is a practical limit on how small the bits can be made. Additionally, modern memory devices have several other shortcomings

which could be amended through substantial changes to their functionality.

Part of the difficulty of this engineering problem lies in the many differing criteria for effective memory, all of which must be optimized for an ideal solution. First, it should be possible to quickly and easily read stored information, with a very low error rate; second, it should be possible to quickly and efficiently write information without risking introducing errors into the data, using a small amount of power; thirdly, it should be possible to store a large quantity of information in a small physical space; and finally, the method of data storage should be robust enough that information is not lost with the passage of time. This final goal will be of particular concern within this thesis, and we will wish to distinguish between memory systems that satisfy or do not satisfy this goal. Volatile memory storage systems quickly lose the information they contain when unpowered. This might be acceptable for storage of information that is only needed while computations are ongoing, but is ineffective for long-term storage. Non-volatile memory systems, on the other hand, continue to hold their information without power, potentially forever. Modern computer RAM is typically volatile, as nonvolatile dense data storage systems typically have long read and write times[1].

At the moment, no practical solution exists that satisfies all four of the above requirements. To rectify this problem, engineers have separated memory into two types – volatile memory that can provide short read and write times (standard RAM), and non-volatile memory with long read and write times (hard drives, such as modern solid state drives). Data needed for active computations or operations

can be stored in the volatile memory and accessed quickly at need, and the end results can be selectively saved to long-term storage in the non-volatile memory.

The core problem with non-volatile memory lies in the fact that it is difficult to store electrical signals. Electrical currents tend to dissipate quickly, and non-homogeneous charge distributions are difficult to maintain without huge energy expenditure. Information that is stored electrically therefore may be lost if power is not supplied to the device. Magnetic information storage provides a potential solution to this problem. A ferromagnetic material subjected to a strong enough magnetic field will become magnetized along the direction of the field, and retain that orientation even once the field is turned off. Unless some other stimulus acts on the ferromagnet, the magnet will store the information imparted by that magnetic field. Small devices made from ferromagnetic materials then offer a promising solution for non-volatile memory. By magnetizing the material either parallel to, or anti-parallel to some chosen direction, we may store either a one or a zero in the magnet. Then, by making sufficiently small magnets, it is possible to create almost arbitrarily dense non-volatile memory. Hence, magnetic memory provides an opportunity for non-volatile quickly accessible memory. One particularly interesting form of such memory is magnetoresistive random access memory (MRAM).

1.2 Magnetic Tunnel Junctions and Information Storage

We have already established that it is possible to store information in magnets in a nonvolatile way. If those magnets are made very small, we can store information densely. Reading and writing data stored in dense arrays of nanomagnets proves challenging, however, as any magnetic field probe must be small and precise indeed to read the magnetic orientation of a single nanomagnet, and any magnetic field used to write information to such a magnet must be exceptionally localized, so that it does not alter adjacent nanomagnets. It is easy, however, to read the resistance of a single electrical element, and similarly easy to apply voltages to a single circuit element – the infrastructure for such actions is already in place in standard computing. Fortunately, various effects couple magnetic signals with electrical signals. More specifically, magneto-resistance effects allow us to determine aspects of the orientation of a nanomagnet by measuring its electrical resistance[2,3,4,5], and spin currents can be used to modify that orientation[12]. Hence, magnetoresistive random access memory makes use of magneto-resistance to read its state.

Magnetic junctions offer a way to generate large magneto-resistances that can effectively be used to probe the orientation of a magnet. Although there are various types of magnetic junctions, here we will only discuss Magnetic Tunnel Junctions (MTJs), which are particularly well suited to the task. In an MTJ, two magnetic layers are separated by an extremely thin insulating tunnel barrier,

across which charge carriers can tunnel (see Fig. 1.1). Because the barrier is thin (a few nanometers), the probability of tunneling across the barrier is high, and so the resistance across the tunnel junction is not excessively large.

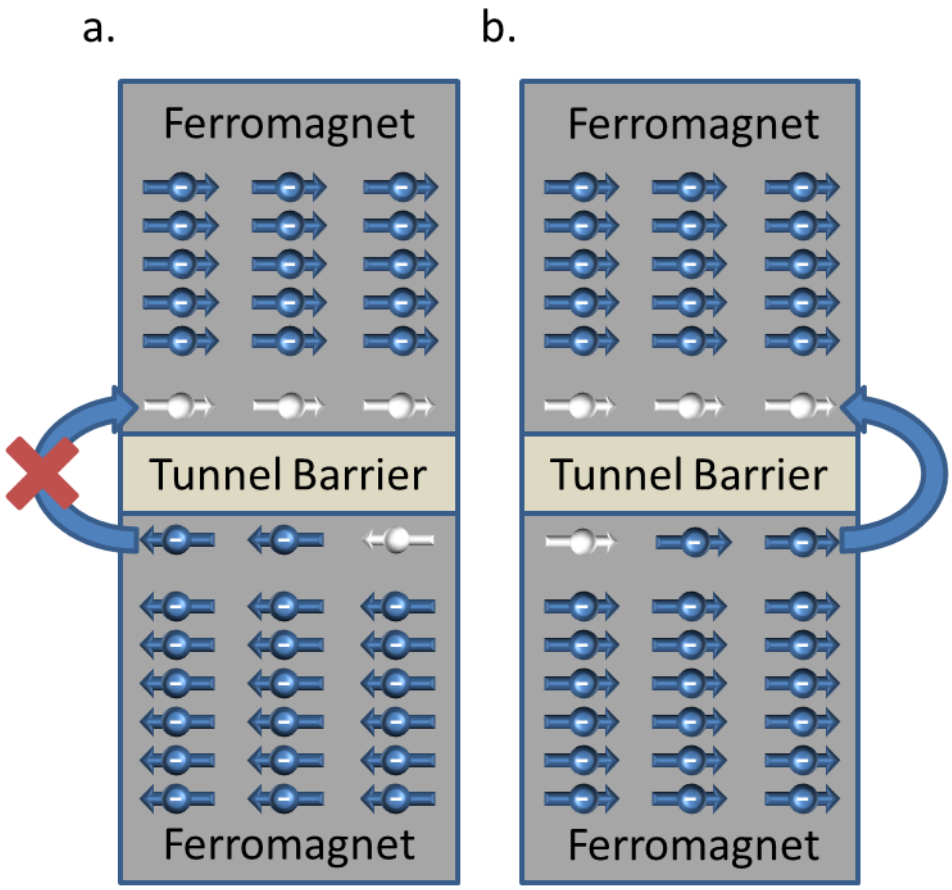

Fig. 1.1. A schematic of a magnetic tunnel junction with in-plane anisotropy in high and low resistance states. Two magnetic layers are separated by an insulating barrier. Charge carriers that tunnel across must move from one available carrier state to another, with their spin matching the state into which they move. In (a), the two magnetic layers are anti-parallel, and so no states are available for charge carriers to tunnel into, and the resistance is accordingly high. In (b), the two magnetic layers are aligned, and so many states are available for charge carriers to tunnel into, and the resistance is accordingly low. MTJs may also have perpendicular magnetic anisotropy, in which the spins point either into or out of the plane of the sample.

In order to pass through the tunnel junction, charge carriers must tunnel directly from an itinerant charge carrier state in the first magnetic layer to an open charge carrier state in the second magnetic layer. Most of the available charge carrier states in the second magnetic layer will have spins oriented in one favored direction – either parallel or antiparallel to its magnetization (in the case of Nickel, Cobalt, and Iron, for instance, the states are parallel[6]), so that charge carriers with magnetic moments approximately parallel to the second magnetic layer's magnetization will cross the barrier more easily than charge carriers with magnetic moments in other directions. However, the first magnetic layer will also have mostly itinerant states for which the spin magnetic moment is parallel or anti-parallel to its magnetization, and so charge currents passing through that material will become spin polarized – their spins will align with the magnetization of the material. Then, if the two magnetic layers are oriented parallel to one another, the resistance will be fairly low, because there are many available states into which the spin polarized charge carriers can tunnel. However, if the two layers are oriented antiparallel to one another, the resistance will be very high, because there are few or no available states into which the charge carriers can tunnel. This effect is known as tunnel magnetoresistance, or TMR[7].

If both magnetic layers are 100% spin polarized, then, when the two magnetic layers are oriented anti-parallel, no charge will tunnel across the barrier[7], and the resistance will be infinitely high. However, it is not necessary to have the

layers be 100% spin polarized and, even if they are not, as is generally the case, high magneto-resistances can be achieved through clever engineering of the barrier and interfaces[8].

1.3 Spin Transfer Torques

Although nanomagnets can be individually manipulated with sufficiently localized magnetic fields, producing such fields proves incredibly challenging, as we have briefly mentioned in the previous section. If the magnetic field is insufficiently strong, it may not properly switch the target magnet. If, on the other hand, it is too strong or insufficiently localized, then it may switch other magnets in close proximity to the target. Computing using electrical signals offers the advantage that electrical currents are locally addressable with relative ease. Just as electrical fields have an addressable analogue in current, however, magnetic fields have an addressable analogue in spin current. Each charge carrier carries an angular momentum, called its spin, and a corresponding magnetic moment proportional to its angular momentum. Spin current may be defined as the collective movement of these spins such that angular momentum is transferred from one location to another. For example, if spin up electrons move in one direction, and spin down electrons move in the opposite direction, we achieve a net flow of angular momentum. These travelling spins can be used to exert torques on

magnetic layers, effectively creating extremely localized magnetic fields on only our desired nanomagnet. Torques exerted in such a way are called spin transfer torques.

Luc Berger first predicted the usage of spin transfer torques for manipulating magnetic domain walls in ferromagnetic materials[9,10], but the effect was not well-considered or understood for some time thereafter. A substantial leap forward was made by Slonczewski, who predicted that current applied through a tunnel junction could be used to manipulate the magnetic state of one of the layers[11,12]. Similar predictions were also made by Berger around the same time[13]. Slonczewski formulated a model for the effects of such a spin torque on a magnetic layer for a macrospin approximation, generalizing the Landau-Lifschitz-Gilbert equation[14], which predicted the behavior of a magnetic material subject to damping, into the now familiar Landau-Lifschitz-Gilbert-Slonczewski (LLGS) equation, which contains additional terms representing the magnetic excitation caused by a spin torque. This equation may be written in the perhaps more familiar form that we will use later on in this thesis.

$$\frac{d\vec{\boldsymbol{m}}}{dt} = -\gamma \vec{\boldsymbol{m}} \times \vec{\boldsymbol{H}}_{tot} + \alpha \vec{\boldsymbol{m}} \times \frac{d\vec{\boldsymbol{m}}}{\boldsymbol{dt}} + \gamma H_{FL} \vec{\boldsymbol{m}} \times \hat{\boldsymbol{\sigma}} + \gamma H_{AD} \vec{\boldsymbol{m}} \times \left(\hat{\boldsymbol{\sigma}} \times \vec{\boldsymbol{m}} \right) \tag{1.1}$$

Now that we have established that spin torques are potentially useful, and that magnetic materials react to them in a predictable way, it becomes practical to consider methods of generating spin transfer torques. Some early experiments with spin transfer torques were conducted in MTJs. One magnetic layer is used to spin

polarize a charge current applied through the junction, as outlined in the prior section. The now spin-polarized charge current flows across the tunnel barrier and into the second magnetic layer, transferring angular momentum from one layer to the other. When the two magnetic layers in the tunnel junction are misaligned, charge carriers attempting to pass through the tunnel barrier may have to reorient in order to find an open state into which they can tunnel. In this case, conservation of angular momentum suggests that the magnetic layer into which the spins have tunneled will experience a torque. This effect allows an MTJ to be constructed with a thick fixed magnetic layer, used to spin polarize an applied current, and a thin free magnetic layer, which can be switched easily by the spin torque from that current. If a current is then applied in the opposite direction, the sign of the spin torque flips, and it is possible to switch the free magnetic layer into the opposite direction, allowing for addressable data writing.

Unfortunately, as outlined in the prior section, an MTJ's state is read by applying current and measuring its resistance. Hence, the method for writing data and reading data are the same. We must therefore be very cautious and engineer a system for which writing to the nanomagnet requires much larger currents than reading it, so that we do not inadvertently switch the state of the magnet while we are reading it. But if we require high writing currents, then write operations use a lot of power, and generate a lot of heat.

MTJs are not the only structures in which spin-polarized charge current can be used to manipulate a magnetic layer. Charge current traveling through a

magnetic material will become spin polarized, and, when incident upon a non-collinear magnetic material, will exert a spin torque even if the two materials are, for instance, separated by a metal. These novel spin torques have proven to be strong enough to effectively switch magnetic materials, both in magnetic tunnel junctions and in other structures[15,16,17].

Unfortunately, as is mentioned above, spin currents generated in this way are accompanied by an undesirable flow of charge current, and charge current dissipates energy. Moreover, there is a limit on the quantity of angular momentum that may be transferred for a given electrical current – even if we can find a magnetic material that 100% spin polarizes the spin current, the ratio between charge and angular momentum will still be constrained by the relation that each charge carrier carries one electron's worth of charge, and one electron spin's worth of angular momentum. Hence, the ratio between the angular momentum imparted by the spin current and the charge current used to carry it is, at best, $\frac{\hbar}{2e}$. For any switching operation, this generates substantial heat dissipation, and wasted energy.

1.4 Spin Hall Effect

All is not, however, lost. There are methods of generating spin current not subject to the above limitation. One such method, the spin Hall effect, was predicted in 1971 by D'yakonov and Perel[18]. This effect has produced a great deal of interest in experimental condensed matter since its initial observations in 2004 and 2005[19,20]. Spin-orbit coupling causes charge carriers moving through a material to undergo spin-dependent deflection in a direction mutually perpendicular to their initial direction of travel and the direction of their spin. Moreover, the sign of this deflection is determined by the sign of the charge carrier's spin. Hence, any charge current moving through a material with large spin-orbit coupling generates a spin current transverse to the charge current direction, with a spin polarization transverse to both the spin and charge current directions. Such a case is depicted in Fig. 1.2.

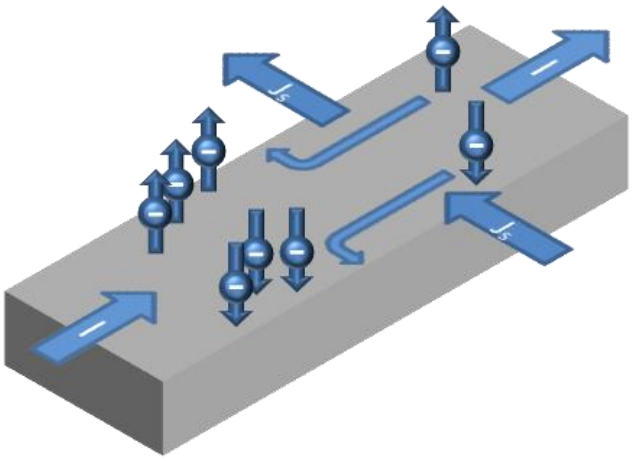

Fig. 1.2. Charge carriers moving through a material undergo spin-dependent deflection, creating an excess of spin-up carriers at one side, and an excess of spin-down carriers at the other side, producing a transverse spin current with no corresponding transverse charge current.

The spin Hall effect broadly refers to spin-dependent deflections stemming from several different sources. The most intuitive source is the intrinsic spin Hall effect, which derives from the intrinsic spin-orbit coupling in the material causing oppositely oriented spins to drift in opposite directions[21,22]. Intuitively, the orbital movement of charge carriers (their velocity) couples to their spin, causing a slight change in their velocity into a direction perpendicular to the initial velocity. More technically speaking, spin-orbit coupling opens small gaps at points in the band structure where a material's bands would ordinarily cross. These avoided crossings generate large Berry phase[23] contributions that create anomalous velocities perpendicular to the initial direction of travel[24].

The spin Hall effect can also be caused by disorder in the material. Impurities can cause spin-dependent scattering events that produce spin-

dependent motion transverse to the initial velocity of the charge carrier[25,26,27]. Broadly, two contributions to the spin Hall effect fall into this category. The first, skew-scattering, refers to a charge carrier scattering off of an impurity and acquiring a spin-dependent change to its velocity. The second, side-jump, refers to a spin scattering off an impurity and, during the collision, acquiring a spin-dependent displacement[28]. It does not necessarily gain any velocity transverse to its initial direction, but repeated spin-dependent displacements cause an overall flow of spin current transverse to the spin's original direction of travel. A diagram illustrating these two effects is shown in Fig. 1.3.

Both of these contributions rely on disorder and impurities in the material. Such contributions have added to the difficulty of creating a consistent picture of the spin Hall effect, because impurities in materials may differ based on growth procedures and conditions. Additionally, the presence of spin currents produced by multiple different sources can make it difficult to create a unifying theory that encompasses all possible contributions to the spin Hall effect.

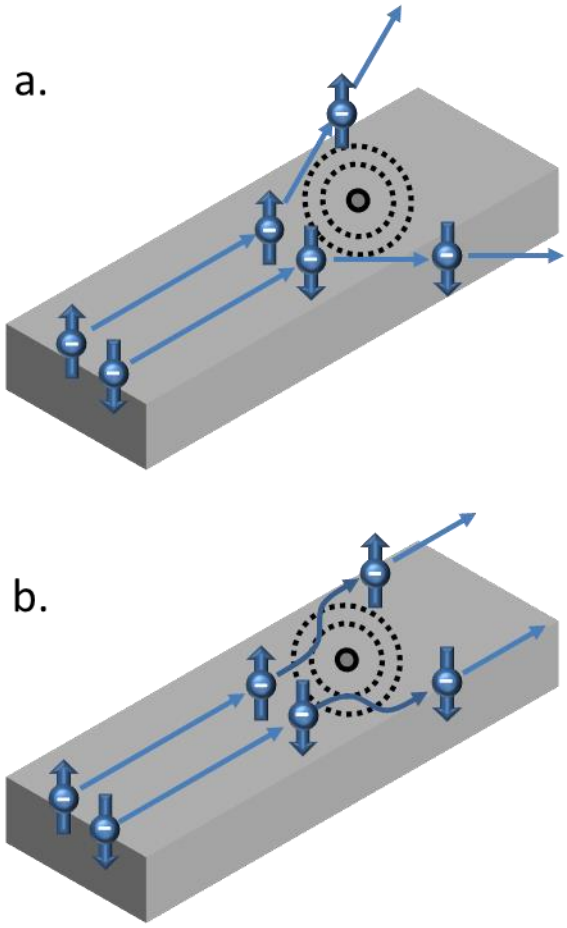

Fig. 1.3. The mechanisms of (a) skew scattering, in which a charge carrier scatters off of an impurity in a direction dependent on the spin of the charge carrier, and of (b) side-jump, in which a charge carrier scatters off of an impurity, acquiring a spin-dependent displacement.

Despite these challenges, the substantial promise held by the spin Hall effect, in addition to our academic curiosity, encourages us to continue to unravel its mystery. As outlined in the prior section, spin transfer torque is a promising avenue for addressable control of nanomagnets, a prospect with wide applications for MRAM and spin computing. Unlike past methods of spin current generation, such as spin polarization via transmission through a ferromagnetic material, the

spin Hall effect has no inherent limit on the ratio of spin current to applied charge current, and so large torques may be generated by small currents. Thus, with a suitable material, switching can be achieved with low currents, and hence low cost and heat generation. Because it is cheap and addressable, the spin Hall effect holds great promise for the future of MRAM.

Before spin transfer torque becomes a practical solution for MRAM systems, spin current generation methods must be honed to produce rapid and efficient switching, which has proven to be a substantial challenge. Materials discovered to date either do not produce spin currents as large as would be ideal, or fall short on other desirable properties, such as conductivity[29,30], or ease of manufacturing[31]. Additionally, for most practical implementations of the spin Hall effect, the geometric considerations of the device define the applied charge current direction, and the direction in which the spin current travels (e.g., along the bar, and vertically into the magnetic material), and so the spin polarization of the generated spin current is completely defined by the geometry of the device. The spin polarization required by most convenient devices is typically designated as the $\hat{y}$ direction, perpendicular to the applied current ($\hat{x}$) and vertical ($\hat{z}$) directions, and generates a spin current that is only capable of exerting in-plane anti-damping torques and out-of-plane field-like torques. This is troubling not only because it limits the versatility of the effect, but also because out-of-plane anti-damping torques are ideal for high-efficiency switching operations. Materials with odd crystal symmetries can generate such spin currents[32], but they are often difficult to produce, and an

ideal material for this purpose has yet to be discovered. Hence, the search for methods to create novel spin torques is an active field, with a great deal of potential yet untapped. However, even without an ideal material, the switching process can be optimized to occur very quickly with reasonably sized currents[33,34]. This success encourages us to continue searching, as the spin Hall effect may soon be able to provide a solution for writing magnetic memory.

Before moving on, it behooves us to discuss how spin-orbit coupling might affect travelling spin currents. Spin currents may consist of a current of spin-up (for some choice of direction designated as ‘up’) charge carriers moving forward, spin-down charge carriers moving backward, or a combination of the two. For a single spin current, spin-up charge carriers move in an opposite direction from spin-down charge carriers, and the sign of their deflection is determined based both on their velocity and on their spin. Therefore, because both the velocity and spin direction are reversed between the spin-up and spin-down carriers, the spin-selective deflection methods described above will deflect spin-up and spin-down carriers both in the same direction, generating a charge current from the applied spin current[35,36]. Because this effect mirrors the spin Hall effect, but in reverse, it is called the inverse spin Hall effect (ISHE).

1.5 Anomalous Hall Effect

The anomalous Hall effect was initially discovered by Edwin Hall in 1881[37] as an electrical effect occurring in magnetic materials. Such materials exhibit a large Hall voltage with curious magnetic field dependence. The size of the Hall voltage grows steeply with low fields, and then saturates fairly quickly. Experiments by Pugh[38] determined that the anomalous Hall resistivity grows with the magnetization – at low fields, the magnetization is pulled linearly out of plane, so there is a steep linear increase, but once the magnetization saturates, so does the anomalous Hall resistivity. This in some sense provided an explanation for the anomalous Hall effect – it grows with the out-of-plane magnetization of the magnetic layer, $V_{AHE} \propto m_z$. However, it did little to explain the cause of the effect.

A contribution to understanding the anomalous Hall effect came from Karplus and Luttinger[39] in 1954. They found that in the presence of spin-orbit coupling and an electric field, the velocity operator has non-zero interband matrix elements that contribute an anomalous velocity perpendicular to the applied electric field. In normal materials, spin-up and spin-down carriers move in opposite directions, and the two velocity terms cancel, producing no net charge current. However, in ferromagnets, spin-up (parallel to the magnetization) carriers outnumber spin-down (anti-parallel to the magnetization) carriers, and this anomalous velocity remains non-zero when integrated over the band structure of the material. Hence, an anomalous Hall conductivity appears. This is known as the

intrinsic contribution to the anomalous Hall effect.

The anomalous Hall effect, like the spin Hall effect, also contains two other substantial contributions – the skew-scattering and side-jump contributions. The skew-scattering component is caused by spin-selective scattering due to disorder in the material[40]. The side-jump contribution comes from a displacement caused by spin-orbit interactions during a scattering event[41]. These contributions are directly analogous to the identically named contributions to the spin Hall effect.

A core element in understanding the anomalous Hall effect is the spin-dependent nature of the deflections. It is no accident that the anomalous Hall effect sources strongly mirror the origins of the spin Hall effect. Both effects stem from spin-orbit coupling, and it seems logical that, given the spin-selective nature of the anomalous Hall effect, a spin current might accompany the anomalous Hall charge current. One could conceive the anomalous Hall current as a charge current generated by a spin current, in a system in which the spins are polarized. A depiction of the anomalous Hall effect is shown in Fig. 1.4. It can be seen, for an out-of-plane magnetization, how the anomalous Hall effect produces both a spin current and a charge current. Because the spin polarization of the charge carriers lies parallel to the magnetization, it follows that the size of the charge current will also scale with the out-of-plane magnetization of the magnetic material, which explains the dependence found by Pugh.

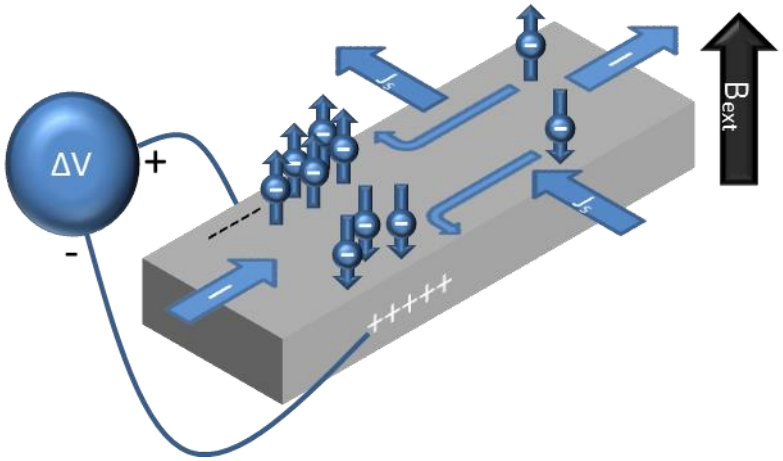

Fig. 1.4. A depiction of the anomalous Hall effect for a perpendicularly oriented magnetic layer. Spin-dependent velocities create a spin current. Excess up-spin charge carriers exist in the material, which causes those spin-dependent deflections to generate a charge current.

If the anomalous Hall effect and the spin Hall effect are analogous, then we would also expect ferromagnets to manifest an effect analogous to the inverse spin Hall effect, in which spin current is spin-selectively deflected to produce charge current. In reality, both of these effects exist. In fact, the ISHE has already been observed in a variety of ferromagnetic materials[42-47], and spin accumulations due to the anomalous Hall effect have also been reported[48,49].

However, the transverse spin currents arising from spin-orbit interactions within a ferromagnet are predicted to have a qualitatively different character than those generated by the SHE in a nonmagnetic heavy metal due to the presence of the strong ferromagnetic exchange field[50,51]. It is not clearly necessary that the spin polarization of the generated spin current should have any special property. As is the case with the spin Hall effect, we expect spins in all directions to be deflected

with the strength and direction of this deflection defined by geometry. However, spins in a ferromagnet precess rapidly around the magnetization (exchange-field) direction, so that any net macroscopic spin current within a ferromagnetic layer should have the spin polarized along $\pm\hat{m}_{\text{source}}$, where $\hat{m}_{\text{source}}$ is the magnetization direction of the source layer. This property lifts many of the geometric restrictions imposed upon potential spin torques generated by the spin Hall effect, which is, as outlined earlier in this chapter, an attractive proposition. In fact, this suggests that it should be possible to reorient the polarization of the spin current produced by spin-orbit interactions within a ferromagnet by reorienting $\hat{m}_{\text{source}}$, to thereby gain the ability to reorient at will both the anti-damping torque and the field-like torque that the spin current applies. Hence, spin current generated by the anomalous Hall effect offers great potential for creating spin torques with arbitrary direction.

Within this thesis, we will make use of the theory of Taniguchi et al. [51], as is covered in more detail in Section 2.5, Derivation of the Second Harmonic Hall Signal for Spin-Orbit Torque Originating from the Anomalous Hall Effect.

CHAPTER 2

HARMONIC HALL TECHNIQUES AND ANOMALOUS HALL SPIN CURRENTS

Many established techniques exist for measuring spin torques produced via the spin-Hall effect (second harmonic Hall[52-55], ST-FMR[29,56,57,58], spin pumping[36,59,60], MOKE[61], for example). However, these established measurement techniques have been formulated for the simple case in which torques are exerted on one magnetic layer only, by spin torques with well-constrained geometric properties, generated via the spin Hall effect. In recent years, these techniques have also been used to measure spin torques with more complicated geometries due to, for instance, broken crystal symmetries[32]. However, if spin currents are to be generated via the anomalous Hall effect in a ferromagnetic layer and detected through a ferromagnetic sensor layer, it becomes important to consider the effects of two magnetic layers instead of one. This concern greatly increases the complexity of any potential measurements, and introduces a host of additional parasitic signals that could plague measurements. Even more troublesome, if we wish to be able to reorient the spin polarization direction of our spin current, and hence, the spin torques generated, then we require a method by which we may control the orientation of the generating ferromagnetic layer, separately from our control of the ferromagnetic sensor layer. This section will detail how such a goal may be achieved by some fairly simple modifications of an ordinary second

harmonic Hall measurement for an in-plane magnetic sensor layer. However, in order to understand the special case of an anomalous Hall generating layer, we first include a treatment of the standard in-plane second harmonic Hall method for in-plane magnetic layers.

2.1 Second Harmonic Hall Method for In-Plane Magnetic Layers

To measure current-induced torques on a magnetic sensor layer (which can arise from either spin currents or an Oersted field) we may use the second-harmonic Hall technique[52-55] in which a low-frequency alternating current is applied to the device and the induced Hall voltage is measured at the second harmonic frequency (see Fig. 2.1). In order to conduct second harmonic Hall measurements for spin Hall torques, it is necessary to construct a sample with a thin-film magnetic sensor layer upon which a spin torque may impinge. For this purpose, it is typical to use a bilayer composed of a spin Hall source layer, often a heavy metal, followed by a magnetic sensor layer, e.g. Platinum/Permalloy or Platinum/$Fe_{60}Co_{20}B_{20}$. The sensor layer may in general have an in-plane or out-of-plane magnetization. However, here we will primarily discuss the measurement for in-plane sensor layers.

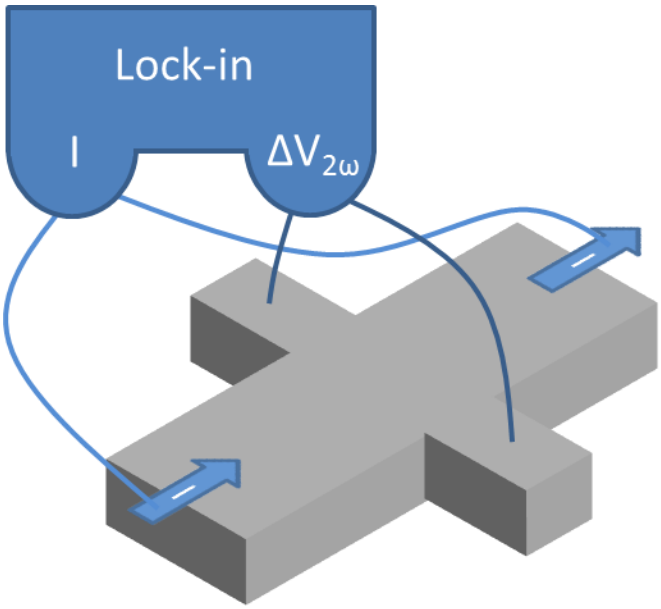

Fig. 2.1. A schematic for the second harmonic Hall measurement. A charge current is applied via a lock-in amplifier to a bar of material, and the transverse Hall voltage at the second harmonic frequency is read by the lock-in amplifier.

In-plane torques correspond to out-of-plane effective magnetic fields (by the right-hand rule) so that they tend to pull an in-plane sensor layer slightly out-of-plane, giving a second harmonic Hall voltage signal on account of mixing between an oscillating anomalous Hall resistance and the oscillating current. Out-of-plane torques, on the other hand, correspond to in-plane effective magnetic fields, and tend to rotate the sensor layer in-plane, giving a second harmonic Hall voltage signal due to mixing between an oscillating planar Hall resistance and the oscillating current. In principle, therefore, the second-harmonic Hall technique can provide measurements of both the in-plane and out-of-plane components of current-induced torque. It can also distinguish anti-damping torques from field-like torques, but one must be careful to distinguish the spin-torque signals from

artifacts associated with non-spin sourced torques, magnetic exchange coupling, or, particularly, thermoelectric effects[54].

For the moment, we will proceed with a general derivation valid for either in-plane or out-of-plane magnetized samples. First, we must note that the spin polarization of spin currents generated by the spin Hall effect is, as discussed in the Spin Hall Effect section, $\vec{\sigma} = \hat{y}$, where $\hat{y}$ is the in-plane direction perpendicular to the applied current direction. Second, we note that for an in-plane magnetic layer, the magnetic sensor layer quickly saturates in the direction of the applied magnetic field. Then, at any point, in the absence of torques, $\vec{m} \| \vec{H}$. For an out-of-plane layer, on the other hand, the magnetization points primarily out of the plane of the sample, and the effect of an in-plane applied magnetic field will be to compete against the out-of-plane anisotropy and pull the layer slightly into the plane of the sample. The orientation of the sensor layer's in-plane component may be reoriented by reorienting the in-plane magnetic field.

We begin with the LLGS equation. It is then possible to quantitatively derive the effects of small spin torques on a magnetic layer. We will here denote the size of the effective field produced by the field-like torque as H_{FL} and that produced by the anti-damping torque as H_{AD}.

$$\frac{d\vec{\boldsymbol{m}}}{dt} = -\gamma \vec{\boldsymbol{m}} \times \vec{\boldsymbol{H}}_{tot} + \alpha \vec{\boldsymbol{m}} \times \frac{d\vec{\boldsymbol{m}}}{dt} + \gamma H_{FL} \vec{\boldsymbol{m}} \times \hat{\boldsymbol{\sigma}} + \gamma H_{AD} \vec{\boldsymbol{m}} \times \left(\hat{\boldsymbol{\sigma}} \times \vec{\boldsymbol{m}} \right) \tag{2.1}$$

For a relatively slow-varying oscillating signal, we may set each of the above time derivatives to zero. Then, for small spin torques relative to the applied magnetic

field, the magnetic sensor layer will be parallel to an effective field, $\vec{\boldsymbol{H}} - m_z H_k \hat{\boldsymbol{z}} - H_{FL}\hat{\boldsymbol{\sigma}} - H_{AD}\hat{\boldsymbol{\sigma}} \times \hat{\boldsymbol{m}}$, where H_k is the magnetic anisotropy field of the thin-film sensor layer.

Assuming the standard torques expected from the spin-Hall effect, the field-like torque then causes an in-plane rotation of the sensor layer magnetization Δϕ, which is detected through the planar Hall effect. The anti-damping torque produces an out-of-plane rotation of the magnetization layer Δθ, which is detected through the anomalous Hall effect.

$$R_{XY} = \frac{1}{2} R_{AHE} \cos(\theta) + \frac{1}{2} R_{PHE} \sin^2(\theta) \sin(2\varphi) \tag{2.2}$$

Here, θ and ϕ denote the polar and azimuthal angles of the sensor layer magnetization, respectively. We define ϕ such that at ϕ=0, the magnetization lies parallel to the applied current direction. We are interested in the case for which the magnetic sensor layer is oriented in the plane of the sample. Accordingly, at this point, we will assume that our sensor layer is magnetized in-plane, setting $\theta = \pi/2$, such that the change in the Hall resistance due to the spin-orbit torques is

$$\Delta R_{XY} = R_{PHE} \cos(2\varphi)\Delta\varphi - \frac{1}{2} R_{AHE} \Delta\theta .$$

Then, we will assume that we observe standard spin Hall field-like and anti-damping torques, which allows us to replace $\hat{\sigma}$ with $\hat{y}$, defined as before to be the in-plane direction perpendicular to the applied current. We then have an effective field $\vec{\boldsymbol{H}} - m_z H_k \hat{\boldsymbol{z}} - H_{FL}\hat{\boldsymbol{y}} - H_{AD}\hat{\boldsymbol{y}} \times \hat{\boldsymbol{m}}$. With this assumption, and for an in-plane sensor

layer, we may simplify further to $\vec{\boldsymbol{H}} - m_z H_k \hat{\boldsymbol{z}} - H_{FL}\hat{\boldsymbol{y}} + H_{AD}\cos(\theta)\hat{\boldsymbol{z}}$, producing

$\Delta\varphi = \frac{H_{FL}^0 \cos(\varphi)}{|H_{tot}|}$ and $\Delta\theta = \frac{H_{AD}^0 \cos(\varphi)}{|H_{tot}| + H_k}$.

As can be seen above, the in-plane torque competes with both the magnetic anisotropy field H_k of the magnetic sensor layer and the applied magnetic field H, to give a second-harmonic signal amplitude $\propto \frac{\cos(\varphi)}{(H_k + |H|)}$, and because $H_k >> |H|$ for most field ranges relevant to the experiment, the magnitude of the second-harmonic Hall signal due to the anti-damping torque is approximately $\propto \frac{1}{(H_k)}$, which should be small and approximately independent of the magnitude of applied magnetic field for a fixed field orientation near $H = 0$. The size of the signal does depend on the orientation of the sensor layer, which modifies the size of the torque as the applied magnetic field is rotated, but introduces no dependence on the size of the magnetic field, assuming no rotation occurs. For the usual case of an anti-damping in-plane torque, flipping the magnetization direction of the sensor layer changes the sign of the deflection (due to the angular dependence), so that the final second-harmonic Hall signal should have a sign change near $H = 0$ upon reversal of our low-coercivity CoFeB layer, and should otherwise be flat as a function of swept magnetic field (Table 2(a)).

Out-of-plane torques, on the other hand, correspond to in-plane effective fields, causing an in-plane rotation of the sensor layer's magnetization that is

detected through mixing with the planar Hall resistance, $\propto \frac{\cos(2\varphi)\cos(\varphi)}{|H|}$. The in-plane effective field competes only with the applied magnetic field. The size of the sensor layer deflection is inversely proportional to the applied field, and we expect a second-harmonic Hall signal whose magnitude diverges as $1/|H|$. For a field-like out-of-plane torque, reversing the sensor layer magnetization direction changes the sign of the second harmonic signal, so that the signal should flip sign as the field is swept through zero to reorient the low-coercivity sensor layer (Table 2(c)). Once again, there is angular dependence, but this angular dependence only causes a sign flip when the magnetization switches, and yields no other applied magnetic field dependence, provided no rotation occurs.

As mentioned in the introduction to this chapter, for unusual materials it has been seen that the spin Hall effect can also create out-of-plane anti-damping torques and in-plane field-like torques, so it becomes useful to address each of these cases. For an in-plane field-like torque, we find identical field-behavior as for an in-plane anti-damping torque, except that the torque has one fewer factor of $\vec{m}$, and so does not switch sign when the magnetization flips, leaving a constant field-dependence (Table 2(b)). For an out-of-plane anti-damping torque, on the other hand, an in-plane effective field is created, producing a signal proportional to $1/|H|$, as with out-of-plane field like torques, but the additional factor of $\vec{m}$ adds a sign change as the sensor magnet switches, producing a final signal with a divergence but no sign change as the applied field passes through zero (Table

2(d)). All of the entries in Table 2 assume that the spin-current-induced torque is nonzero and approximately independent of magnetic field in the range near H=0; if the magnitude of the torque depends on field there will be deviations (as discussed below, when deriving the analogous case for anomalous Hall spin currents) from the ordinary $1/|H|$ dependence for out-of-plane torques and *H*-independent behavior for in-plane torques.

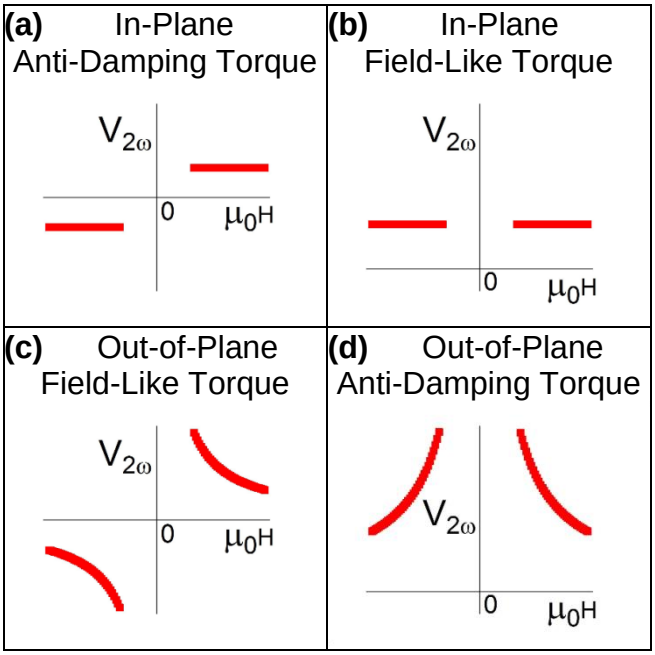

Table 2. Predicted second harmonic Hall signals resulting from various forms of spin torque acting on a ferromagnetic sensor layer with in-plane magnetization for applied fields near zero. These results assume that the spin torque is nonzero and does not vary strongly with applied magnetic field near *H* = 0.

It is now useful to note that the angular dependence of these spin Hall torque signals will be relevant when choosing an experimental geometry. If, for example, the magnetic field is applied in the y-direction, then the spin polarization

of the spin current lies parallel to the sensor layer magnetization, and both the traditional spin Hall field-like and anti-damping torques produce no effect. For a traditional spin Hall measurement, this would be inconvenient. However, in this document, we are more concerned with non-conventional torques generated by a magnetic anomalous Hall spin source layer, which do not fall to zero when the magnetic field is applied perpendicular to the current direction. Hence, this geometry becomes convenient for us, as it eliminates the possibility that we are observing conventional torques, ensuring that any torques we observe are non-conventional. The benefits of our chosen geometry will be described in more detail in the next section.

2.2 Controlling a Magnet through the Exchange Bias

To probe the effects of an anomalous Hall spin torque, we wish to independently control the orientation of two different in-plane magnetic layers – the sensor layer and the source layer. For this purpose, we choose to exchange bias the source layer using an anti-ferromagnetic material. It is therefore useful to briefly discuss the properties of anti-ferromagnetic materials as they contrast to those of ferromagnetic materials.

In ferromagnetic materials, it is energetically favorable for the spins within the material to align with one another, creating large magnetic fields and hysteresis

loops due to the self-reinforcing properties when all of the spins line up. Above a certain temperature, the thermal energy is enough to overcome this desire, and the ferromagnet loses its order. On cooling below that temperature, the spins will once again line up with one another. The spins in the material, however, also wish to align with any external magnetic field applied to the system. Because all of the spins lie in the same direction, it is hugely energetically favorable for the entire magnet to align with the applied magnetic field, and so even in the presence or relatively small magnetic fields, ferromagnets will tend to re-orient themselves.

In anti-ferromagnetic materials, on the other hand, it is energetically favorable for the spins to align anti-parallel to one another. Once again, above a certain temperature, in this case called the Néel temperature, this ordering will be destroyed. The spins will become disordered, and, upon cooling, will once again choose an orientation and align parallel with it. This produces no net magnetic field. It remains energetically favorable for one spin to align with an external applied magnetic field, but because their anti-ferromagnetic ordering causes half of them to be anti-parallel to the other half, there is no energetically favorable state that allows the spins to all align with the external field. Hence, anti-ferromagnetic ordering is fairly robust against applied magnetic fields. In order to modify the anti-ferromagnet's ordering direction, it is then necessary to heat it above its Néel temperature, and, by defining an ordering access while it is cooling down, it is possible to choose its orientation.

We are here concerned more with the properties of an interface between a

thin anti-ferromagnetic layer and a thin ferromagnetic layer. In this case, the high exchange coupling present between the ferromagnet magnetic moments and the anti-ferromagnet magnetic moments will make it energetically favorable for the topmost spins in the anti-ferromagnet to align with the ferromagnet's magnetization. If we create a sample consisting of a ferromagnet grown on an anti-ferromagnet, and heat it up, we may destroy the ordering of the anti-ferromagnet. Then, by cooling it in an applied magnetic field, we may set the ordering direction such that the top layer of the anti-ferromagnet aligns itself parallel to the applied field direction. Because the anti-ferromagnet's ordering is so robust against applied fields, however, this new orientation locks in once the material cools below the Néel temperature. The top layer of the anti-ferromagnet remains in the set direction regardless of what fields are applied, whereas the top ferromagnet moves freely with field. A schematic of an exchange biased system, with a depiction of the state of the ferromagnet and anti-ferromagnet at various points in its hysteresis loop, is shown in Fig. 2.2.

In many experimental cases, including that discussed in this thesis, we use an uncompensated anti-ferromagnetic material, in which the magnetic moments in the top layer do not all align. However, some fraction of the magnetic moments do align, which yields an exchange bias field.

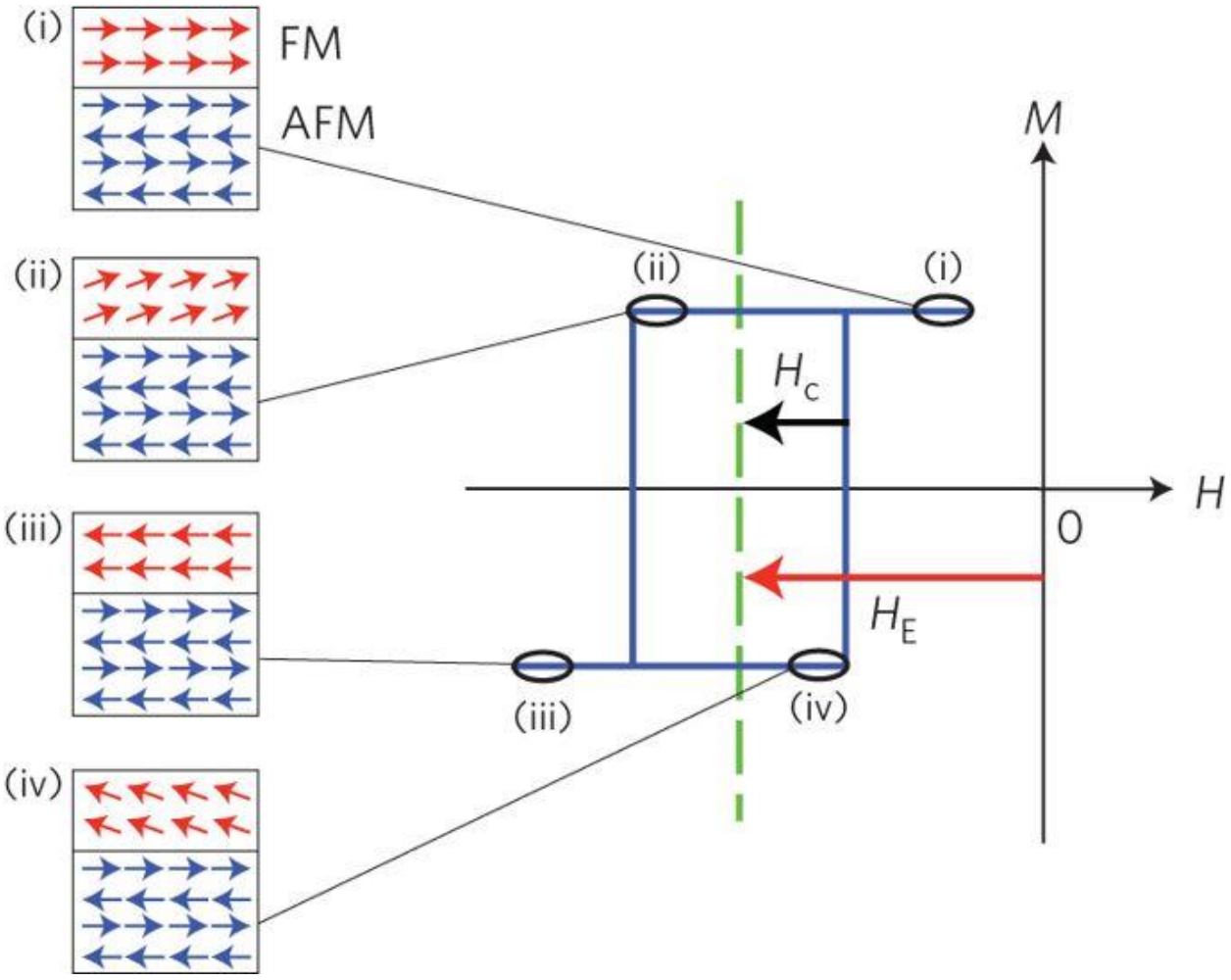

Fig. 2.2[62]. A schematic of an exchange biased ferromagnetic layer and the state of the ferromagnet and anti-ferromagnet as magnetic field is swept through the system's hysteresis loop.

The end result of this system is that the anti-ferromagnet now exerts an effective field, in this thesis designated as H_{EB}, on the ferromagnet layer that points in the direction we set during cooling. Hence, in the absence of a magnetic field, the ferromagnet will align with that direction, and, when magnetic field is applied, it will compete with the exchange bias field, and the ferromagnet will follow

the sum of the two fields.

2.3 A Special Geometry and How to Use It

With the sensor magnetic layer free and the source layer exchange biased, it is possible to control the magnetic layers in different directions as we wish. If we choose a sufficiently clever geometry for our measurement, it may also be possible to sweep the magnetic field and observe the reorientation of the spin current caused by the reorientation of the source layer magnetization, as the externally applied magnetic field competes against the exchange bias.

Because of these concerns, and, moreover, because of the presence of potential spin torque signals and parasitic signals occurring in both layers, it is important to carefully select a special geometry for our measurements. This has been alluded to in the previous chapter, and, in the following sections describing our specific methods of dealing with parasitic signals, will be described in more detail. Hence, as this thesis proceeds, it will become increasingly clear why we have chosen the experimental geometry we describe here.

To best distinguish whether the magnetic source layer gives rise to a spin-orbit torque that depends on the orientation of the source layer moment, we wish to choose a measurement configuration for which the torques arising from both the current-generated Oersted field and also any conventional spin Hall effect must be

zero. Such a geometry eliminates any ordinary signals, such that any resulting spin torque observed must be novel. This is notably true if we sweep the applied magnetic field perpendicular to the current flow direction, and also align the exchange bias parallel to the current direction, so that the low-coercivity sensor layer is quickly saturated perpendicular to the current (for $\left|\mu_0 H\right|$ greater than approximately 0.01 Tesla), while the angle, φ_{Source}, of the source layer magnetization rotates slowly away from the exchange bias direction with increasing field magnitude. In this geometry the sensor moment is parallel to the spins that would be created by any conventional spin Hall effect, so that there can be no conventional spin Hall torque. However, this geometry affords further benefits, as will be alluded to in future sections, by requiring that many of our potential parasitic signals will be zero.

The downside of such a complex system is that in order to understand the system, we must be certain we understand the orientation and behavior of its component magnetic layers under our various experimental conditions. Hence, we will proceed with discussing the primary technique that allows us to do this – first harmonic Hall measurements.

2.4 First Harmonic Hall Measurements

In order to understand the second harmonic Hall behavior of a system, it is beneficial to understand the behavior of the ferromagnetic layers and their magnetizations under various applied magnetic fields. It is possible to understand some of the properties of the magnetic layers by analyzing ordinary first harmonic Hall measurements taken via lock-in amplifier. The setup for such measurements is quite simply a standard Hall signal measurement, in which current is applied along a bar, and the Hall voltage across the bar is measured via lock-in amplifier. For this measurement, the first harmonic Hall signal for a magnetic layer with arbitrary magnetization direction described by the angles θ and ϕ is

$$V_H^{1f} = \frac{1}{2} IR_{AHE} \cos(\theta) + \frac{1}{2} IR_{PHE} \sin^2(\theta) \sin(2\varphi). \quad (2.3)$$

By observing the first harmonic Hall signal, it is then possible to understand the position of the relevant magnetic layers. For our system, we have two different magnetic layers, and the first-harmonic Hall signal will include contributions from both layers:

$$V_H^{1f} = \frac{1}{2} IR_{AHE,Sensor} \cos(\theta_{Sensor}) + \frac{1}{2} IR_{PHE,Sensor} \sin^2(\theta_{Sensor}) \sin(2\varphi_{Sensor}) \quad (2.4)$$

$$+ \frac{1}{2} IR_{AHE,Source} \cos(\theta_{Source}) + \frac{1}{2} IR_{PHE,Source} \sin^2(\theta_{Source}) \sin(2\varphi_{Source}) \ .$$

Here, $R_{PHE,Sensor}$ and $R_{PHE,Source}$ refer to the contributions to the planar Hall resistance

due to the Sensor and Source layers, respectively. $R_{AHE,Sensor}$ and $R_{AHE,Source}$ are likewise the contributions to the anomalous Hall resistance due to the sensor and source layers. In other sections of this work, R_{PHE} and R_{AHE} are used to refer to the planar Hall resistance and anomalous Hall resistance, respectively, of the relevant material that is being discussed. For the purpose of quantitative analysis, it will be necessary to distinguish the two, and know separately the size of the two R_{PHE} terms in particular. These values may also be extracted from the size of the first harmonic Hall measurements, under appropriate magnetic field conditions.

We will begin with the case of primary interest, the first harmonic Hall signal for an in-plane magnetic layer, for which the magnetic field is applied in the plane of the sample. Then, the resulting first harmonic Hall signal will be

$$V_H^{1f} = \frac{1}{2} I R_{PHE} \sin(2\varphi) + C_{offset}.$$

For a magnetic layer that is in-plane and not exchange biased, such as in our sensor layers, the magnet quickly saturates in the direction of the applied magnetic field, and φ corresponds to the direction of the applied field. On the other hand, we find a more interesting result for an exchange biased ferromagnetic layer. The magnetic field is here assumed to be also in-plane, and, as outlined in the previous section, applied perpendicular to the exchange bias direction. It is not difficult to generalize for a magnetic field that is not perpendicular to the exchange bias direction, but it is also not particularly interesting. As a result, we find a first harmonic Hall signal of the following form.

$$V_H^{1f} = \frac{1}{2} IR_{PHE} \sin\left(2\arctan\left[\frac{H}{H_{EB}} \right] + 2\varphi^0 \right) + C_{offset}, \quad (2.5)$$

where C_{offset} is a constant offset voltage, H_{EB} is the exchange bias field amplitude, and φ^0 is the angle of the exchange bias direction relative to the applied current direction. By measuring the first harmonic Hall voltage under various in-plane magnetic field conditions, it is then possible to extract the size of the planar Hall resistance, as well as the exchange bias and the angle of the exchange bias with respect to the applied current direction.

Next, we will discuss the first harmonic Hall signal for such a layer when the magnetic field is applied in the direction out of the plane of the sample. We will assume that the applied magnetic field and exchange bias field are both much smaller than the magnetic anisotropy field, i.e. $H, H_{EB} \ll H_k$ and therefore that we may make a small angle approximation, and the exchange bias field may be ignored. This results in a first harmonic Hall voltage of $V_H^{1f} = \frac{1}{2} IR_{AHE} \frac{H}{H_k}$. Measuring this signal then allows us to extract the value of the magnetic anisotropy field and anomalous Hall resistance.

It should be further noted here that the presence of more than one magnetic layer in a sample can often cause confusion between the layers from each magnetic material. However, by making clever use of the different properties of the two layers, it may be possible to distinguish them. In particular, if one layer is exchange biased, it will be possible to separate the effects. Otherwise, one can

construct control samples that are identical save that one of the magnetic layers is not included. In this case, the magnetic properties of that single layer may be measured in the absence of the other, and should be approximately the same as in the primary sample with which we are concerned.

2.5 Derivation of the Second Harmonic Hall Signal for Spin-Orbit Torque Originating from the Anomalous Hall Effect

Now that we have described an ordinary second harmonic Hall experiment, and outlined the behavior of the first harmonic Hall effects, seeing how they may be used to measure the position of our magnetic layers as they respond to external fields, we will adapt the ordinary second harmonic Hall method to our unique case – anomalous Hall spin currents with controllable spin orientation.

In order to comprehend the effects of an anomalous Hall spin current of arbitrary spin polarization direction, we should first consider the angular dependence of each torque we might expect to see. For the purposes of this thesis, we will consider only the anomalous Hall analogue of the traditional anti-damping and field-like torques. By controlling the orientation of the spin polarization, we can unlock sufficiently rich physics and sufficiently versatile torques, without considering more exotic torques from, for instance, low-symmetry crystal structures. More importantly, the simple nature of the materials under

discussion in this thesis make more complicated torques irrelevant. To obtain a quantitative model for the anomalous Hall analogues to anti-damping and field-like torques, we compare to the theory of Taniguchi et al.[51], in which spin-orbit coupling within the ferromagnetic source layer generates a transverse spin current with polarization $\vec{\sigma} \propto (\hat{y} \bullet \hat{m}_{AHE}) \hat{m}_{AHE}$, where $\hat{m}_{AHE}$ is a unit vector along the spin source layer magnetization direction, and $\hat{y}$ is the in-plane direction perpendicular to the applied charge current. Intuitively, we can think of this as a projection of the ordinary SHE spin current onto the magnetization direction. The above statement may be translated into two essential assumptions regarding the anomalous Hall spin current. First, we assume that the spin current $\hat{\boldsymbol{\sigma}}$ is parallel to the source-layer magnetization $\hat{m}_{AHE}$. In this case, the spin torques retain the same form as for the spin Hall effect, $\gamma H_{FL} \vec{\boldsymbol{m}} \times \hat{\boldsymbol{\sigma}}$ and $\gamma H_{AD} \vec{\boldsymbol{m}} \times (\hat{\boldsymbol{\sigma}} \times \vec{\boldsymbol{m}})$, the form of field-like and anti-damping torques, respectively. $|H_{FL}|$ and $|H_{AD}|$ characterize the strength of the field-like and anti-damping spin-orbit torques. Second, we have assumed that the size of the anomalous Hall spin current scales with the in-plane component of the spin polarization perpendicular to the applied current direction, or that $H_{FL} = H_{FL}^{0} \sin(\theta_{AHE}) \sin(\varphi_{AHE})$ and $H_{AD} = H_{AD}^{0} \sin(\theta_{AHE}) \sin(\varphi_{AHE})$. Here, φ_{AHE} is the angle between the applied current direction and the generating anomalous Hall layer magnetization, and θ_{AHE} is the angle between the generating anomalous Hall layer magnetization and the out-of-plane axis. Our model for control of these angles will be discussed later in this document. Note that we have conducted a

minor change in labeling, now using the subscript AHE to refer to the anomalous Hall source layer, rather than the label 'source,' used previously.

Making use of these forms for the anomalous Hall spin torques, we use the Landau-Lifshitz-Gilbert-Slonczewski (LLGS) equation in the macrospin approximation to determine the magnetization orientation of our magnetic sensor layer ($\vec{m}$), adapting the calculation of Hayashi et al.[55]. In the presence of arbitrary spin-current-induced field-like and anti-damping torques, the time-dependent LLGS equation may be written

$$\frac{d\vec{\boldsymbol{m}}}{dt} = -\gamma \vec{\boldsymbol{m}} \times \vec{\boldsymbol{H}}_{tot} + \alpha \vec{\boldsymbol{m}} \times \frac{d\vec{\boldsymbol{m}}}{dt} + \gamma H_{FL} \vec{\boldsymbol{m}} \times \hat{\boldsymbol{\sigma}} + \gamma H_{AD} \vec{\boldsymbol{m}} \times \left(\hat{\boldsymbol{\sigma}} \times \vec{\boldsymbol{m}} \right). \qquad (2.6)$$

We will analyze the case in which the sensor layer magnetization is in-plane, and the external magnetic field $\vec{\boldsymbol{H}}$ is also applied in-plane. For low-frequency second harmonic Hall measurements, a quasi-steady state condition applies, meaning that the time derivative terms in Eq. (S1) can be taken to be zero. The CoFeB magnetization then follows the total effective field, and since the CoFeB layer is approximately isotropic within the sample plane, $\vec{m}$ should be parallel to $\vec{\boldsymbol{H}} - m_z H_k \hat{\boldsymbol{z}} - H_{FL} \hat{\boldsymbol{\sigma}} - H_{AD} \hat{\boldsymbol{\sigma}} \times \hat{\boldsymbol{m}}$, where H_k is the magnetic in-plane anisotropy field of the thin-film sensor layer. Up to this point, the derivation is identical to the case for ordinary SHE torques. However, we will not here assume that the spin polarization is perpendicular to the current, but rather that it follows the magnetization of the source layer. We will consider here the torques that are dominant for the case in which the spin source layer's magnetization lies in the

plane of the sample, retaining the azimuthal angular dependence at first for generality. As a result, the dominant effect of the field-like spin-orbit torque is to rotate the sensor-layer magnetization within the sample plane by an angle

$$\Delta\varphi_{Sensor} = \frac{H_{FL}^{0}\sin^{2}\left(\theta_{AHE}\right)\sin\left(\varphi_{AHE}\right)\sin\left(\varphi_{Sensor}-\varphi_{AHE}\right)}{\left|H_{tot}\right|} \tag{2.7}$$

relative to its value in the presence of the applied magnetic field but with no spin-orbit torque. Here, H_{tot} designates the total magnetic field due to, for instance, an applied field or an exchange bias field. This expression assumes that $\left|H_{FL}^{0}\right| \ll \left|H\right|$. Similarly, the anti-damping torque arising from the anomalous Hall effect should deflect the sensor layer magnetization perpendicular to the sample plane,

$$\Delta\theta_{Sensor} = \frac{H_{AD}^{0}\sin^{2}\left(\theta_{AHE}\right)\sin\left(\varphi_{AHE}\right)\sin\left(\varphi_{Sensor}-\varphi_{AHE}\right)}{\left|H_{tot}\right|+H_{k}} . \tag{2.8}$$

These deflections will alter the Hall resistance, R_{XY}, which can have contributions from the anomalous Hall effect and the planar Hall effect:

$$R_{XY} = \frac{1}{2}R_{AHE}\cos\left(\theta_{Sensor}\right)+\frac{1}{2}R_{PHE}\sin^{2}\left(\theta_{Sensor}\right)\sin\left(2\varphi_{Sensor}\right). \tag{2.9}$$

Assuming a sensor layer with in-plane anisotropy (so that in the absence of spin-orbit torques, $\theta_{Sensor} = \pi/2$), the change in the Hall resistance due to the spin-orbit torques is

$$\Delta R_{XY} = R_{PHE}\cos(2\varphi_{Sensor})\Delta\varphi_{Sensor} - \frac{1}{2}R_{AHE}\Delta\theta_{Sensor} . \tag{2.10}$$

At this point, we will assume that the anomalous Hall spin current generating layer

has a magnetization that is also oriented in-plane, such that $\sin(\theta_{AHE})=1$. After mixing with the oscillating applied current $I\sin\omega t$, the oscillating planar Hall resistance will produce a second harmonic signal

$$V_{\mathrm{H}}^{2f}=-\frac{1}{2}IR_{\mathrm{PHE}}\cos(2\varphi_{Sensor})\frac{H_{FL}^{0}\sin(\varphi_{AHE})\sin(\varphi_{Sensor}-\varphi_{\mathrm{AHE}})}{|H_{tot}|}+\frac{1}{4}IR_{AHE}\frac{H_{AD}^{0}\sin(\varphi_{\mathrm{AHE}})\sin(\varphi_{Sensor}-\varphi_{\mathrm{AHE}})}{|H_{tot}|+H_{k}} \tag{2.11}$$

Here I is the applied current, R_{PHE} is the planar Hall coefficient of the multilayer due to the sensor layer, and φ_{Sensor} is the angle between the current and the magnetic field. The *H* dependence of V_{H}^{2f} comes from the *H* dependence of j_{FeGd} and the susceptibility term $\frac{1}{|H_{tot}|}$, and $\frac{1}{|H_{tot}|+H_{k}}$ for the field-like and anti-damping torques, respectively. At this point, it is worth mentioning that, while H_{tot} may in general contain contributions from an exchange bias field or other field effects, we are interested in the case where our sensor layer has no exchange bias, and so $H_{tot}=H$. In this case, when $\vec{H}$ is applied in-plane perpendicular to the current direction and the sensor layer magnetization is saturated parallel to this field, $j_{CoFeB}=\pm p/2$, depending on the sign of the applied magnetic field.

We will begin by inspecting the results of the first term, due to the planar Hall effect. For an in-plane ferromagnetic sensor layer, the system is more sensitive to out-of-plane torques than in-plane torques, and, as a result, this first term is likely to be highly important. Using our special geometry for the magnetic sensor layer, this term, associated with the field-like spin-orbit torque via the planar

Hall effect, becomes $V_{\mathrm{H}}^{2f} = \frac{1}{2} I R_{\mathrm{PHE}} \frac{H_{FL}^{0} \sin(\varphi_{AHE}) \cos(\varphi_{AHE})}{|H|}$.

The second term in the right in Eq. (2.11), associated with the anti-damping spin-orbit torque, reduces to $V_{\mathrm{H}}^{2f} = \frac{1}{4} I R_{AHE} \frac{H_{AD}^{0} \sin(\varphi_{\mathrm{AHE}}) \cos(\varphi_{\mathrm{AHE}})}{|H| + H_k}$.

Both of these signals are strongly dependent on the orientation of the generating anomalous Hall layer's magnetization. As described in section 2.3, A Special Geometry and How to Use It, above, we are in particular interested in a case where the spin source layer is exchange biased in an in-plane direction parallel to the applied current direction, and for which the magnetic field is applied perpendicular to the current direction. It is not difficult to generalize this derivation to include arbitrary directions of exchange bias and applied magnetic field, but it is also not relevant, and so will be omitted. It is essential to take into account that the direction of the exchange bias on the source layer ($\varphi_{\mathrm{AHE}}^{0}$) in any real experiment will be slightly misaligned from the current direction due to experimental uncertainties, so that $\varphi_{\mathrm{AHE}} \approx \varphi_{\mathrm{AHE}}^{0} + \tan^{-1}(H / H_{\mathrm{EB}})$. Here, H_{EB} is the magnitude of the exchange bias field. We are particularly interested in the case where $\varphi_{\mathrm{AHE}}^{0}$ is close to, but not quite, zero. If φ_{AHE}^{0} were exactly zero, the spin torque would go to zero for *H*=0. However, in the presence of a small misalignment angle, the torque will be non-zero at zero field, and the divergence predicted due to the $\frac{1}{|H|}$ susceptibility term will appear in the data. Additionally, such a misalignment will result in an asymmetric shape to

the field-dependent second harmonic Hall measurement. Assuming a small value for the misalignment, and reasonable values for H_k and H_{EB}, we may model each of these signals. The resulting prediction is shown in Fig. 2.3.

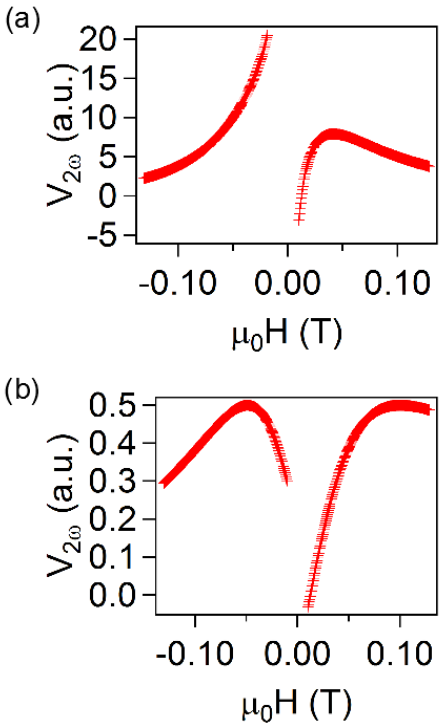

Fig. 2.3. The predicted second harmonic Hall signal as a function of applied magnetic field due to (a) the oscillating planar Hall resistance in the sensor layer induced by a field-like anomalous Hall torque of controllable spin polarization, with a divergence near zero field because it is an out-of-plane torque and (b) the oscillating anomalous Hall resistance in the sensor layer induced by an anti-damping anomalous Hall torque of controllable spin polarization, showing an increase and fall-off in signal due to the controllable spin polarization, but no divergence, because it is due to an in-plane torque.

While our above analysis made use of the assumption that the spin polarization of the generated spin current is in-plane, such an assumption is not

necessary. For a spin polarization with an out-of-plane component, the field-like torque will produce an out-of-plane rotation of the sensor layer magnetization,

$$\Delta\theta_{Sensor} = \frac{H_{FL}^{0}\cos(\theta_{AHE})\sin(\theta_{AHE})\sin(\varphi_{AHE})}{|H_{tot}| + H_{k}}. \quad (2.12)$$

The anti-damping torque, on the other hand, will produce an in-plane rotation

$$\Delta\varphi_{Sensor} = \frac{H_{AD}^{0}\cos(\theta_{AHE})\sin(\theta_{AHE})\sin(\varphi_{AHE})}{|H_{tot}|}. \quad (2.13)$$

Hence, an anomalous Hall effect spin current generated in a layer with magnetization partially in the out-of-plane direction generates an out-of-plane anti-damping torque and an in-plane field-like torque, both of which are novel torques. Moreover, as discussed earlier, out-of-plane anti-damping torques are potentially very useful for magnetic switching operations for practical applications such as MRAM. Hence, these other torques may also prove interesting to study.

2.6 Potential Parasitic Signals for Second Harmonic Hall Measurements with Two Magnetic Layers

Unfortunately, the in-plane second harmonic Hall technique is plagued with parasitic signals. Fortunately, our choice of geometry described in section 2.3, A Special Geometry and How to Use It, eliminates many such parasitic signals. However, it is still necessary to consider carefully each possible source of parasitic

signals and, if they cannot be eliminated altogether, to account for them in our final measurements, so that we can be certain that our measured signal reflects a spin torque generated through the anomalous Hall effect rather than, e.g., some well-understood thermo-electric effect. It is additionally possible that the two magnetic layers could couple to one another. This problem can be mitigated by including a spacer layer between the two magnets in order to magnetically isolate them, but even so, some coupling could exist. In this case, we might expect the movement of one of the magnetic layers to couple into the other magnetic layer and induce rotations that could cause a parasitic signal. Such a parasitic signal is especially dangerous because it requires the presence of both magnetic layers to manifest, and so might be confused with some more exotic effect. It is, therefore, also important to consider possible signals generated by this coupling.

Signals due to Oersted Torques:

An applied current generates an Oersted magnetic field perpendicular to the current direction. In our geometry, this aligns with the $\hat{y}$ direction, or $90°$. This effect causes an out-of-plane torque, rotating the magnetization of the magnetic layer in plane. Oersted torques are primarily relevant for in-plane sensor layers, the case in which we are interested. However, assuming such a geometry isn't necessary, and we will maintain generality here. Assuming a small Oersted field

$h_{Oe} \ll H$, the magnetic layer's magnetization will be rotated by $\Delta\varphi = \frac{H_{Oe}\cos(\varphi)}{H_{tot}}$.

This rotation couples through the planar Hall effect to generate a second harmonic Hall signal for a general magnetic layer. $|H_{tot}|$ here refers to the total in-plane magnetic field, potentially including exchange bias or applied fields, as follows.

$$V_{\mathrm{H}}^{2f} = -\frac{1}{2} I R_{\mathrm{PHE}} \sin^2(\theta)\cos(2\varphi)\frac{H_{Oe}\cos(\varphi)}{|H_{tot}|} \tag{2.14}$$

It is easy enough to eliminate the Oersted torque from a free magnetic sensor layer. We simply apply our magnetic field parallel to the $\hat{y}$ direction, perpendicular to the current. In this case, the Oersted field lies parallel to the magnetization, and no Oersted signal is generated. The reader will note that, conveniently, this is the geometry we have outlined above as a convenient choice in the section 2.3, A Special Geometry and How to Use It.

Though we may easily eliminate the Oersted signal on our sensor layer, it is still possible for our spin source layer, which is also magnetic, to act as a sensor and contribute a planar Hall signal due to the Oersted magnetic field. In this case, it is not so easy to eliminate the signal, as the source layer is reoriented by the competition between the applied magnetic field and the exchange bias during field sweeps. In this case, we have an exchange biased sensor layer with applied magnetic field perpendicular to the exchange bias direction, for which we find

$$V_{\mathrm{H}}^{2f} = -\frac{1}{2} I R_{\mathrm{PHE}} \sin^2(\theta)\cos(2\varphi)\frac{h_{Oe}\cos(\varphi)}{\sqrt{H^2 + H_{EB}^2}}. \tag{2.15}$$

This signal cannot be easily eliminated via geometry. Accordingly, it becomes necessary to understand the size and form of this signal. It is possible to measure the size of the planar Hall resistance, and likewise the size of the exchange bias, through first harmonic Hall measurements as discussed above, in section 2.4, First Harmonic Hall Measurements. Accordingly, if we are able to estimate the size of the Oersted magnetic field, it is possible to fully predict the consequences of this parasitic signal. It is additionally possible to engineer a system for which this signal is small, by controlling the size of the Oersted field.

To estimate the Oersted field in a system, we approximate our layers as infinite sheets of current, which contribute a magnetic field $H = \frac{\mu_0 I}{2w}$, where w is the width of the bar, and I is the total current through the layer. Layers below the relevant sensor layer contribute an Oersted field in the $-\hat{y}$ direction, while layers above the relevant sensor layer contribute a field in the $\hat{y}$ direction. If the current in layers above and below the sensor layer are made to be approximately equal, this signal can be made small. Alternatively, the signal can be accounted for by calculating its size and including the result when analyzing the final data from the second harmonic Hall measurements. One can also pursue both goals, by making the signal small, and also accounting for whatever signal is left over.

Signals due to the Anomalous Nernst Effect:

Thermal parasitic signals are an important consideration in any magnetic

system, but even more so for a two-magnet system, and especially for materials with high anomalous Hall effects. A potential anomalous Nernst signal generated by a vertical thermal gradient in either sensor layer could contribute to the measured second harmonic Hall signal. Electrons diffusing along a thermal gradient create a current flow, which couples through the anomalous Hall effect to induce a transverse voltage. The voltage induced is of the form $V_{ANE} \propto \vec{m} \times \vec{\nabla} T$. We will assume that the thermal gradient, ∇T, is out-of-plane[54,63-65]), which is the dominant effect in our system. The temperature gradient has a component proportional to the square of the current, $I = I \sin(\omega t)$, which can appear on the second harmonic, $\Delta T = \Delta T_0 + \Delta T_1 \sin^2(\omega t)$. Then, we have an anomalous Nernst signal $V_{ANE}^{2f} \propto m_x \Delta T_1 = \Delta T_1 \sin(\theta)\cos(\varphi)$.

For an in-plane free sensor layer, the convenient geometry we have chosen above forces the anomalous Nernst parasitic signal to be zero. However, if the field is even slightly misaligned, this signal may be expected to contribute to the second harmonic Hall voltage, so care must be taken to account for this. In such a case, the signal produced has no field dependence except for a sign change when the magnetic layer flips direction.

An in-plane exchange biased layer gives us more trouble. We may expect a Nernst contribution that changes with the angle of the exchange biased layer, $V_{ANE}^{2f} \propto \Delta T_1 \cos(\varphi_{AHE})$. In this case, not only will the signal still exist, but its dependence as the applied magnetic field is swept will be complicated by the

competition between the applied magnetic field and the exchange bias field. It is, therefore, necessary to make a measurement of this contribution using a control sample.

On the possibility of indirect current-induced torques due to coupling between the ferromagnetic layers:

It is possible in principle that there could be a current-induced reorientation of one magnetic layer from either spin-orbit torques or current-induced Oersted torques, which through coupling between the two magnetic layers could induce an indirect current-induced torque on the second layer. In order to understand these signals and their relevance to a system with two magnetic layers, it is useful to derive the consequences of such an effect. For the purposes of this derivation, we will consider only our intended experimental system – first, we will assume that the two magnetic layers are oriented in the plane of the sample, the case of interest to us. Second, we will assume that one of the layers is exchange biased, such that the two layers are not aligned directly with one another; once again, this is the case of relevance to us. Finally, we will treat the case for which the exchange biased layer is rotated by a torque (in practice, this will most likely be the Oersted torque), and the rotation affects the sensor layer through the exchange field.

The interlayer exchange coupling between two magnetic layers may manifest as an energy term of the form $-J\cos(\varphi)$ (bilinear coupling), with J the strength of the coupling and φ the angle between the two layers. When

considering the effect of such an energy contribution on one magnet's orientation due to the other, this term acts identically to a magnetic field oriented parallel to the direction of the second magnet's magnetization, with strength related to the coupling between the two layers. The coupling here may be positive (in which case the two layers align ferromagnetically) or negative (the two layers then couple anti-ferromagnetically). Let us assume, then, that the magnetic coupling acts as an effective field with strength H_{ex}, which will be negative if the coupling was negative. In this case, we expect a rotation of the orientation of the sensor layer given by

$$\Delta\varphi_{Source} = \arctan\left(\frac{H_{ex}\sin\left(\varphi_{AHE}-\varphi_{Sensor}\right)}{H+H_{ex}\cos\left(\varphi_{AHE}-\varphi_{Sensor}\right)}\right), \tag{2.15}$$

where H_{ex} denotes the size of the exchange field, and φ_{Sensor} is the orientation of the sensor layer in the absence of the exchange field. If, as for the special geometry we have described earlier in this section, the magnetic field is applied perpendicular to the applied current direction, then the orientation of the magnetic sensor layer will be $\varphi_{Sensor} = \pm 90°$, and we have

$$\Delta\varphi_{Source} = -\arctan\left(\frac{H_{ex}\cos\left(\varphi_{AHE}\right)}{H+H_{ex}\sin\left(\varphi_{AHE}\right)}\right). \tag{2.16}$$

This rotation is small for high field values, but it becomes relevant at low fields. It does not, however, relate to the applied current, and so does not generate a second harmonic Hall signal. If some torque, generated by the Oersted field, for example, causes oscillations in φ_{AHE}, those oscillations may affect the orientation

of the sensor layer through the exchange coupling. Hence, for some small change $\Delta\varphi_{AHE}$ in the orientation of the source layer, we find,

$$\Delta\left(\Delta\varphi_{Source}\right) = -\arctan\left(\frac{H_{ex}\cos\left(\varphi_{AHE}+\Delta\varphi_{AHE}\right)}{H+H_{ex}\sin\left(\varphi_{AHE}+\Delta\varphi_{AHE}\right)}\right)+\arctan\left(\frac{H_{ex}\cos\left(\varphi_{AHE}\right)}{H+H_{ex}\sin\left(\varphi_{AHE}\right)}\right). \quad (2.17)$$

When deriving our primary second harmonic Hall model, and indeed, for most of our other parasitic signals, we have used the assumption that the applied magnetic field is large compared to, for example, the effective field produced by the various torques. In this case, however, we cannot make that assumption, as the coupling between the source layer and sensor layer is the most relevant for low applied magnetic fields. We may, however, assume small $\Delta\varphi_{AHE}$. This approximation yields

$$\Delta\left(\Delta\varphi_{Source}\right) = -\frac{\Delta\varphi_{AHE}H_{ex}\left(H_{ex}+H\sin\left(\varphi_{AHE}\right)\right)}{H_{ex}^2+2H_{ex}H\sin\left(\varphi_{AHE}\right)+H^2}. \quad (2.18)$$

This rotation couples through the planar Hall effect to generate a second harmonic Hall voltage

$$V_{\mathrm{H}}^{2f} = \frac{1}{2}IR_{\mathrm{PHE}}\cos\left(2\varphi_{Sensor}+2\Delta\varphi_{Sensor}\right)\frac{\Delta\varphi_{AHE}H_{ex}\left(H_{ex}+H\sin\left(\varphi_{AHE}\right)\right)}{H_{ex}^2+2H_{ex}H\sin\left(\varphi_{AHE}\right)+H^2}. \quad (2.19)$$

We have not here concerned ourselves with the source of $\Delta\varphi_{AHE}$. In order to apply this formula to a specific case, it will be necessary to substitute in an expression for the rotation of the anomalous Hall source layer due to the effect being considered. If, as is the most likely to be relevant, the rotation is produced by

an Oersted field, $\Delta\varphi_{AHE} = \frac{H_{Oe}\cos(\varphi_{AHE})}{\sqrt{H^2 + H_{EB}^2}}$. In this case, if the value of the planar Hall resistance, exchange bias, and exchange field are known, then it is possible to estimate the size of the signal produced. Each of these things may be measured relatively easily through known techniques that are covered within the methods section of this thesis. Using values we have extracted from our own measurements on a two-ferromagnet multilayer, we have constructed a practical estimate for such a signal, shown in Fig. 2.4. For low exchange field values, however, the signal only becomes relevant for very small applied fields, and so is not of especial concern if an appropriately sized spacer layer is used between the two magnetic layers.

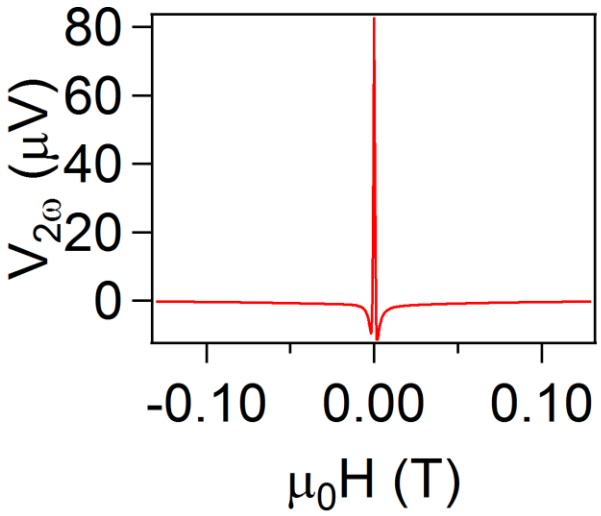

Fig 2.4. The predicted signal due to exchange coupling between the magnetic layers, using experimentally determined realistic values for the size of the exchange coupling.

CHAPTER 3

SECOND HARMONIC HALL METHOD FOR ANOMALOUS HALL SPIN TORQUES: METHODS AND RESULTS

To measure spin current generated by the anomalous Hall Effect, it is necessary to create physical samples corresponding to the system we have modelled theoretically. In order to do this, we must select the relevant materials and deposit them on a substrate. Afterwards, we must construct Hall bars from the relevant material, and connect them to an experimental setup by which we may conduct the measurements. It is also necessary to characterize and understand the properties of our materials if we wish to quantitatively model their behavior. In this chapter, we will discuss the choices made and the methods used to measure reorientable spin currents generated by the anomalous Hall effect.

3.1 Materials and Fabrication

We must choose materials for the following purposes, the need for which has already been discussed in the prior chapters: an exchange biasing antiferromagnetic layer; a source magnetic layer; a spacer layer; and a sensor magnetic layer. In addition, it is necessary to use a capping layer that prevents

oxidation of the top relevant material layer. The most important choices of material for our measurement are the choice of source and sensor layer. The source layer determines the size of the spin current, while the sensor layer determines the size of the planar and anomalous Hall effects.

We choose an alloy of iron and gadolinium, $Fe_{95}Gd_5$, as our spin-source material because rare earth ferromagnetic alloys have the potential for efficient spin-current generation due to the potentially large spin-orbit coupling of rare earth metals – in particular, past research[66] has found that certain iron-gadolinium alloys may exhibit a strong anomalous Hall effect. Unfortunately, later research has shown gadolinium to have a relatively small spin Hall effect[67], which suggests that another material choice might be preferable for future studies.

For our magnetic sensor layer, we choose $Co_{40}Fe_{40}B_{20}$, a fairly standard choice for an in-plane magnetic layer. We choose this material because of its large anomalous Hall effect that potentially allows us to observe both out-of-plane and in-plane torques. For an exchange biasing layer, we use $IrMn_3$, an antiferromagnet which has often been used to effectively exchange bias materials in the past, both by ourselves and by other research groups[68,69,70]. Based on measurements of the exchange bias and Neel temperature across a range of film thicknesses, we determine that a 10 nm thick $IrMn_3$ layer provides a Néel temperature significantly above room temperature and a reasonably sized exchange bias. For our spacer layer, we use hafnium, a material which, when grown by our group, seems to have little spin Hall effect[52,67,71,72]. We note here that other groups have detected a larger

spin Hall effect in hafnium than that grown in our chamber[73,74,75]. The hafnium spacer is selected for the minimum size, 2 nm, that can be used such that the FeGd and CoFeB magnetic layers do not couple to one another significantly. It behooves us to make this layer as thin as possible because, as will be discussed later, some spin current will be dissipated in the hafnium. Finally, we use a hafnium capping layer to prevent oxidation of our other materials.

Our thin film stack thus comprises a 10 nm IrMn layer, followed by a 4 nm $Fe_{95}Gd_5$ (henceforth FeGd) source layer, a 2 nm Hf spacer, and a 2 nm $Co_{40}Fe_{40}B_{20}$ sensor layer (henceforth CoFeB) capped with 3 nm of Hf. Our films are grown on sapphire wafers via DC magnetron sputtering. The FeGd layer is grown from an alloyed FeGd target in the stated proportions.

After growth, the samples are then patterned into 120 μm by 20 μm Hall bars using optical lithography and ion milling (see Fig. 3.1 for an illustration of our fabrication process), with devices placed at angles ranging from zero to 90 degrees, in fifteen degree steps. We then use optical lithography and a lift-off process to deposit 5 μm voltage probes onto the Hall bars. Subsequently, we anneal the samples at 420 K for one hour in a 0.2 T in-plane magnetic field to set the exchange bias direction of the IrMn layer parallel to the orientation of the 0 degree devices. An image of our die, as well as a zoomed image of a single device, is shown in Fig. 3.2. Our measurements are taken using a device with applied current parallel to the exchange bias direction, as outlined in section 2.3, A Special Geometry and How to Use It.

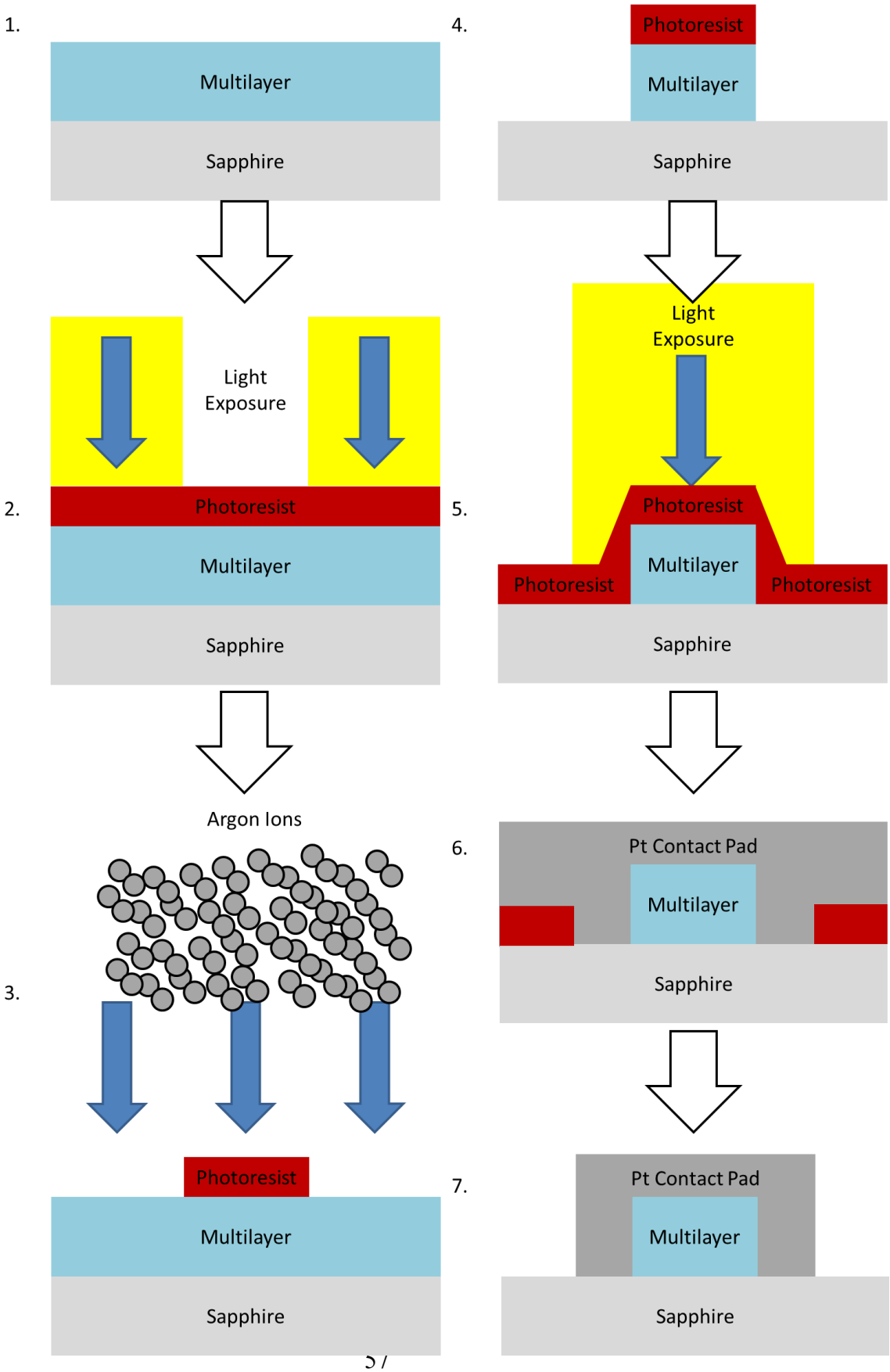
1.
Multilayer
Sapphire
2.
Light
Exposure
Photoresist
Multilayer
Sapphire
3.
Argon Ions
Photoresist
Multilayer
Sapphire
4.
Photoresist
Multilayer
Sapphire
5.
Light
Exposure
Photoresist
Photoresist
Multilayer
Photoresist
Sapphire
6.
Pt Contact Pad
Multilayer
Sapphire
7.
Pt Contact Pad
Multilayer
Sapphire

Fig 3.1. A depiction of our fabrication process for our samples. In step 1, a multilayer is prepared on a sapphire substrate. In step 2, photoresist is applied and patterned using a stepper. In step 3, the exposed photoresist is removed by a developer and ion milling is done using argon ions to define Hall bars. In step 4, the sample is prepared for its second step of processing. In step 5, new photoresist is applied to the sample, and the sample is once again patterned using a stepper. In step 6, platinum contact material is deposited onto the sample. In step 7, the photoresist is stripped, removing the excess materials and defining contacts via a lift-off process. An in-depth description of these processes and their parameters is detailed in Appendix A, Detailed Description of Fabrication Processes.

To rule out potential experimental artifacts, we prepared two control samples in identical ways: (i) IrMn(10 nm)/Hf(2 nm)/ $Co_{40}Fe_{40}B_{20}$ (2 nm)/Hf(3 nm) and (ii) IrMn(10 nm)/FeGd(4 nm)/Hf(3 nm), the first having no $Fe_{95}Gd_5$ layer, and the second having no CoFeB layer. They are also patterned via ion mill and lift-off, and then annealed in nearly the same direction (any potential misalignments in our annealing could be different between the samples). We confirmed that these show essentially the same magnetic properties when grown separately as when grown together.

a.

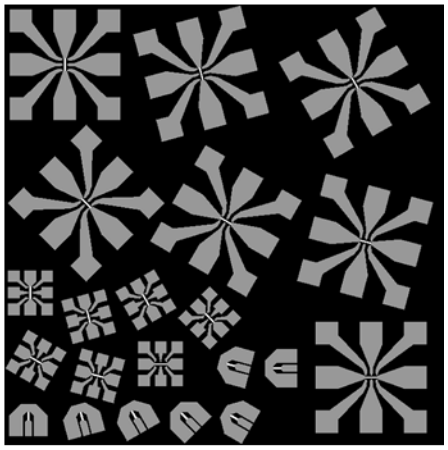

b.

Fig. 3.2. (a) An example picture of one of our dies, containing Hall bars at a variety of different angles, with both large and small contact pads. (b) An example image of a Hall device, with small contact pads. The Hall bar is shown in white, and the contact pads in grey.

3.2 Sample Properties, Characterization, and First Harmonic Hall Measurements

Before we characterize our sample, it is important to understand our characterization methods and how our materials react to external applied magnetic fields. As has already been described, our magnetic materials are oriented in the plane of the sample, with the magnetic field being applied perpendicular to the exchange bias direction, also within the plane of the sample. The exchange bias from IrMn acting on the FeGd layer then allows us to control the angle between the magnetic moments of the CoFeB and FeGd layers, and therefore to study whether the orientation $\vec{\sigma}$ of the spin current produced by current flow in the FeGd layer depends on the FeGd moment orientation. The soft CoFeB layer saturates along even weak external fields, whereas the FeGd layer rotates smoothly from the exchange bias direction to the applied field direction as the strength of the external field is increased. A diagram illustrating the geometry used, as well as the expected behavior of the anomalous Hall spin torque, is shown in Fig. 3.3 (a).

If, on the other hand, the magnetic field is applied parallel to the exchange bias direction, the exchange biased magnetic layer will exhibit a hysteretic switching that has been shifted away from zero-field by the exchange bias field exerted by the IrMn layer, while the free sensor layer will switch rapidly very close to zero applied magnetic field. It is possible to measure this hysteresis loop via Vibrating Sample Magnetometry (VSM). Figure 3.3 (b) shows a VSM measurement

of the magnetization of our unpatterned film stack as a function of a magnetic field applied in the sample plane parallel to the set exchange bias. When increasing the magnetic field from zero, we see first the in-plane magnetization switching of the low-coercivity CoFeB sensor layer. This is followed at higher fields by the more gradual switching of the strongly exchange biased FeGd layer. This gives us an estimate for the size of the exchange bias, and allows us to confirm that both magnetic layers are oriented in the plane of the sample.

Increasing the exchange bias of the IrMn layer increases the exchange bias field that competes with the applied magnetic field, and hence allows us to increase the applied magnetic field range over which we may observe the changing spin polarization direction. The exchange bias of IrMn grows with decreasing temperatures, so to increase the exchange bias, we performed all measurements at cryogenic temperatures, approximately 30 K. Accordingly, it is important to characterize our sample at 30K. Conveniently, the VSM hysteresis loop in Figure 3.3 (b) was taken at 30K.

Next, we wish to know the resistivity of each of our material layers, so that we can determine the size of the current flowing through each material. These 30 K resistivities may be measured by creating samples identical to our original samples, with only the relevant material layer absent. By then treating the different layers as parallel resistors, we may extract the resistance of the layer about which we care. As an example, supposing we wished to know the resistance of the CoFeB layer, we might grow a stack IrMn/FeGd/Hf/Hf, and measure its resistance,

$R_{Control}$, and compare that with the resistance of the full stack, R_{Stack}, to find the resistance, and hence the resistivity of only the CoFeB layer, as follows.

$$\frac{\rho L}{wt} = R_{CoFeB} = \left[\frac{1}{R_{Stack}} - \frac{1}{R_{Control}} \right]^{-1} \tag{3.1}$$

Here, L denotes the length and w the width of the device being measured, and t denotes the thickness of the CoFeB layer. ρ is the resistivity of the CoFeB layer. In this way, we determine the resistivities of the materials to be 209 ± 20 μΩcm (IrMn), 64 ± 8 μΩcm (FeGd), 80 ± 20 μΩcm (Hf), and 94 ± 35 μΩcm (CoFeB).

We take our primary measurements in a Quantum Design Physical Property Measurement System (PPMS), with the temperature controlled to be 30K. It is possible to conduct some of our characterization by measuring the first harmonic Hall voltage on some samples at the same time as we conduct our primary measurements. Such measurements allow us to confirm that our experimental parameters are as expected, and that the sample is behaving as we predict. For example, we use sample holders capable of rotation out of plane, such that the field may be applied at a controlled angle, which gives us some freedom in what first harmonic Hall measurements we can take, and allows us to apply an in-plane field, but allows the possibility of experimental misalignments leading to an out-of-plane field component. Accordingly, we place our primary sample in the system at the same time as a control layer with only a CoFeB sensor layer. Because the anomalous Hall effect is sensitive to applied out-of-plane fields, we may use first harmonic Hall measurements on the CoFeB to detect the out-of-plane field. Using

this, we then calibrate the system to eliminate any stray out-of-plane fields for our primary measurements. We therefore now discuss how the first harmonic Hall measurements may be used for other characterizations, as well.

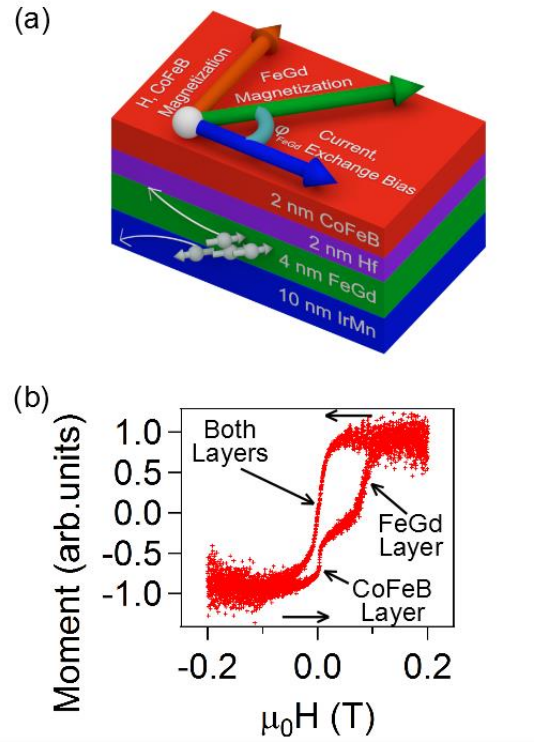

Fig. 3.3. (a) Schematic of the device geometry. (b) Magnetization of an unpatterned IrMn/$Fe_{95}Gd_5$/Hf/$Co_{40}Fe_{40}B_{20}$/Hf multilayer at 30 K measured using vibrating sample magnetometry, showing the exchange-biased switching of the FeGd layer with high coercivity, and the low-coercivity switching of the CoFeB layer.

For our primary sample, IrMn/FeGd/Hf/CoFeB/Hf, the FeGd and CoFeB layers contribute meaningfully to the first harmonic Hall signal. We take simultaneous first harmonic Hall measurements during our primary second

harmonic Hall signal, under identical field conditions. This allows us to fit the first harmonic Hall data to extract the orientation of the FeGd source layer as an external field is applied. The measured data, with an accompanying fit to the theory described in Section 2.4, i.e., $V_H^{1f} = \frac{1}{2} I R_{PHE,FeGd} \sin\left(2\arctan\left[\frac{H}{H_{EB}}\right] + 2\varphi_{FeGd}^0\right) + C_{offset}$, is shown in Fig. 3.4.

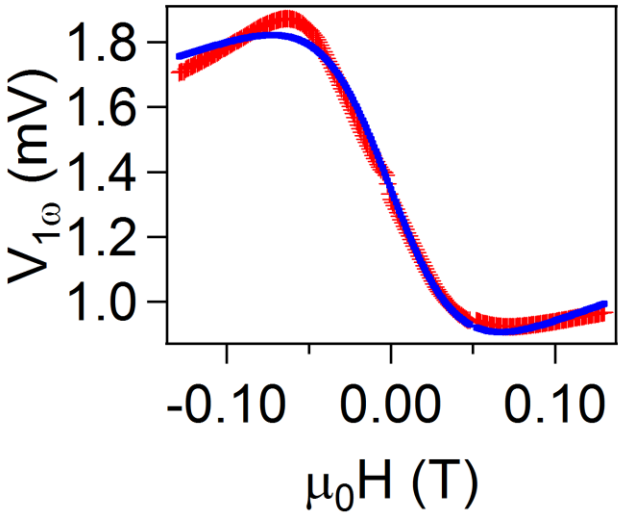

Fig. 3.4. First harmonic Hall data (red markers) taken at 30 K, with the exchange bias parallel to the current and the magnetic field perpendicular to the exchange bias. The value of the FeGd layer exchange bias is extracted from the fit (blue line) to the planar Hall signal.

In particular, the fit allows us to extract the value of the exchange bias (with much more accuracy than the prior VSM data did), the size of the FeGd planar Hall resistance, and, in principle, the misalignment angle, φ_{FeGd}^0, of the FeGd exchange bias direction with respect to the applied current. Unfortunately, this fit is rather

insensitive to the misalignment angle, and does not give an accurate estimate of its value. However, we successfully extract the value of the planar Hall resistance and exchange bias from this measurement. We find the exchange bias value to be $\mu_0 H_{ex} = 0.070 \pm 0.001$ at 30K; the value of the planar Hall resistance, and many other parameters, is printed in Appendix B, Fit Procedures and Parameters for Second Harmonic Hall Measurements. We then use the exchange bias value to predict the orientation of the FeGd layer, φ_{FeGd}, as a function of magnetic field, using the model outlined in the previous chapter. We can use this information to predict the expected second harmonic Hall signal due to a spin polarization parallel to that orientation. While the primary aim of this measurement is to find the orientation of the FeGd layer with field, the value of the planar Hall resistance of the FeGd layer also has some relevance; it is not important for the signal generated by the CoFeB layer, but it is necessary in order to calculate the size of the Oersted signal generated in the FeGd layer.

Because the field-like torque generated by the FeGd spin current produces a signal through the oscillating CoFeB planar Hall resistance, it is necessary to measure the planar Hall resistance of the CoFeB layer. It is possible to do this by measuring the first harmonic Hall signal on our primary sample. However, this signal will also include a contribution due to the rotation of the FeGd layer, which will be further complicated by the exchange bias, which prevents the FeGd layer from saturating easily and contributes additional angular dependence to the signal. Hence, it becomes more difficult than anticipated to separate the two. Therefore, to

determine the size of the planar Hall effect in the CoFeB layer, we perform a first-harmonic planar Hall measurement on the IrMn/Hf/CoFeB control sample; we saturate the CoFeB layer with a large magnetic field, and rotate the magnetic field while measuring the Hall signal. This measurement is shown in Fig. 3.5. To apply the result to the full IrMn/FeGd/Hf/CoFeB multilayer, we take care to account for current shunting by correcting the applied current so that the same current flows in the CoFeB layer of the control sample as in the full multilayer. We must take into account the addition of the FeGd layer in the primary sample, as its absence in the control sample will affect the measured Hall resistance. For this calculation, it is important to know the resistance of the relevant layers.

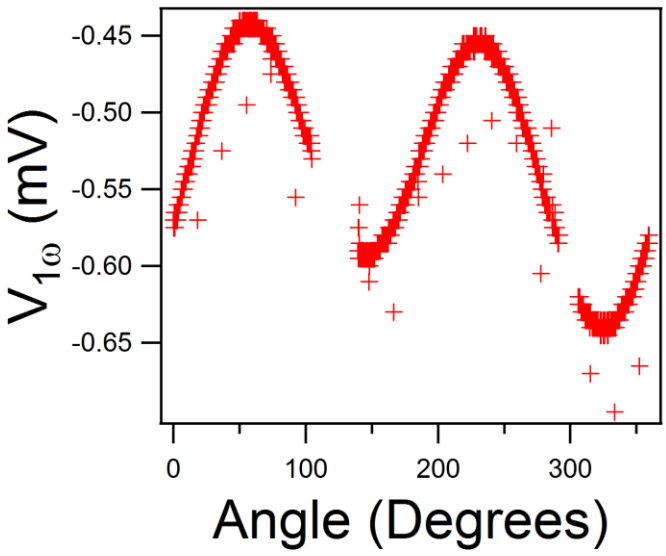

Fig. 3.5. The first harmonic Hall signal of the CoFeB control sample as a function of applied magnetic field angle, for large applied magnetic field.

It will also be important to measure the size of the anomalous Hall effect, as

in-plane torques can be detected through the anomalous Hall effect. As outlined in Section 2.4, First Harmonic Hall Measurements, the first harmonic Hall signal may also be used to extract such values in either CoFeB or FeGd. However, is it nearly impossible to distinguish the effect from the two layers in the full sample. As such, it is necessary to perform this measurement on the IrMn/FeGd/Hf and IrMn/Hf/CoFeB/Hf control samples. The value of the CoFeB anomalous Hall resistance becomes important if we wish to observe anti-damping torques, and, even in their absence, is necessary if we wish to place an upper limit on the size of such anti-damping torques. However, the FeGd layer anomalous Hall resistance is also interesting, because a large anomalous Hall effect might imply substantial spin-orbit coupling, which could correspond to a large spin anomalous Hall effect.

A measurement of the anomalous Hall effect in the IrMn/FeGd/Hf control sample is shown in Fig. 3.6. Electrical current is applied along the Hall bar while an external out-of-plane magnetic field is swept, and the transverse induced voltage is measured. We plot the anomalous Hall resistance in the form V_{AHE} / I, where V_{AHE} is the Hall voltage detected, and *I* is the total current. (Approximately 57% of this current flows within the FeGd layer.) We conduct the same measurements on the CoFeB control sample (Fig. 3.6 (b)), and find that the sign of R_{AHE} is the same as for CoFeB samples. For the FeGd layer, the field is swept to sufficiently high values to observe the beginning of saturation, so that the presence of an exchange bias does not influence the measurement, and that the size of the

anomalous Hall resistance may be obtained: $R_{AHE,FeGd}$ » 3.25 Ω. For our CoFeB layer, the value we care about for characterizing the anti-damping torque is instead $\frac{R_{AHE}}{H_k}$, which may be extracted for low field ranges. Then, we obtain the size of the Hall effect for the CoFeB layer, $\frac{R_{AHE,CoFeB}}{H_k} \approx 25.7$ mV/T.

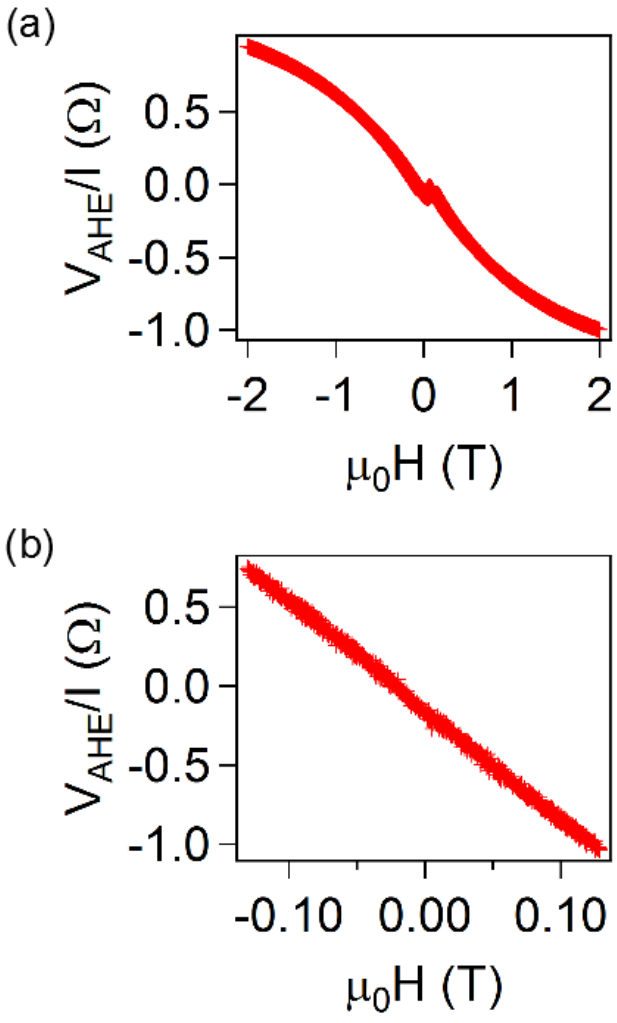

Fig. 3.6. (a) Anomalous Hall resistance measurement at 30 K for the IrMn/FeGd/Hf

control sample, with the applied magnetic field perpendicular to the sample plane. (b) Identical measurement for the CoFeB magnetic layer, with smaller applied magnetic field range. The sign of the anomalous Hall resistance is the same between the FeGd layer and the CoFeB layer.

3.3 Results

Our experimental results in our special geometry for the second harmonic Hall voltage as a function of the applied magnetic field (perpendicular to the applied charge current direction) are shown in Fig. 3.7 (a). We have excluded data for field magnitudes less than 0.01 Tesla from our analysis, because in this regime the CoFeB layer undergoes a spatially non-uniform reversal process that invalidates the macrospin assumption we use to interpret the second harmonic Hall measurements. Additionally, as described above in Section 2.6, an artifact due to coupling between the magnetic layers can also exist in this very low field range. We will exclude the same range of field for all data analyzed below from samples containing the CoFeB layer. We observe in Fig. 3.7 (a) a substantial signal whose magnitude diverges approximately as $1/|H|$ as *H* approaches zero, with a sign change as *H* is swept through 0. This is the signature of an out-of-plane field-like torque (see Table 2 (c) in section 2.1). Because the low-coercivity CoFeB sensor is the only layer that reverses near *H* = 0 (while the FeGd magnetization remains oriented near the exchange bias direction), this behavior indicates that the signal arises from a torque on the CoFeB sensor layer. Unlike the schematic curve

sketched in Table 2 (c), the magnitude of this spin-current-induced torque is not constant, but rather changes as a function of changing field magnitude, and hence as a function of changing j_{FeGd}. This is evident because if the magnitude of the torque were constant, the magnitude of the second-Harmonic hall signal should decrease monotonically with increasing field magnitude as $\mu 1/|H|$, while the data display a distinctly non-monotonic dependence at positive field, with V_{2w} initially increasing and then decreasing as $\mu_0 H$ increases from 0. To quantitatively explain these results, we need a full theory for a reorientable spin polarization second harmonic Hall technique. Fortunately, we have already created such a theory earlier, in section 2.5. Unfortunately, this model does not perfectly replicate our observed results. Qualitatively, it looks quite similar, but quantitatively, it cannot produce a good fit by itself (see Fig. 3.7 (b)).

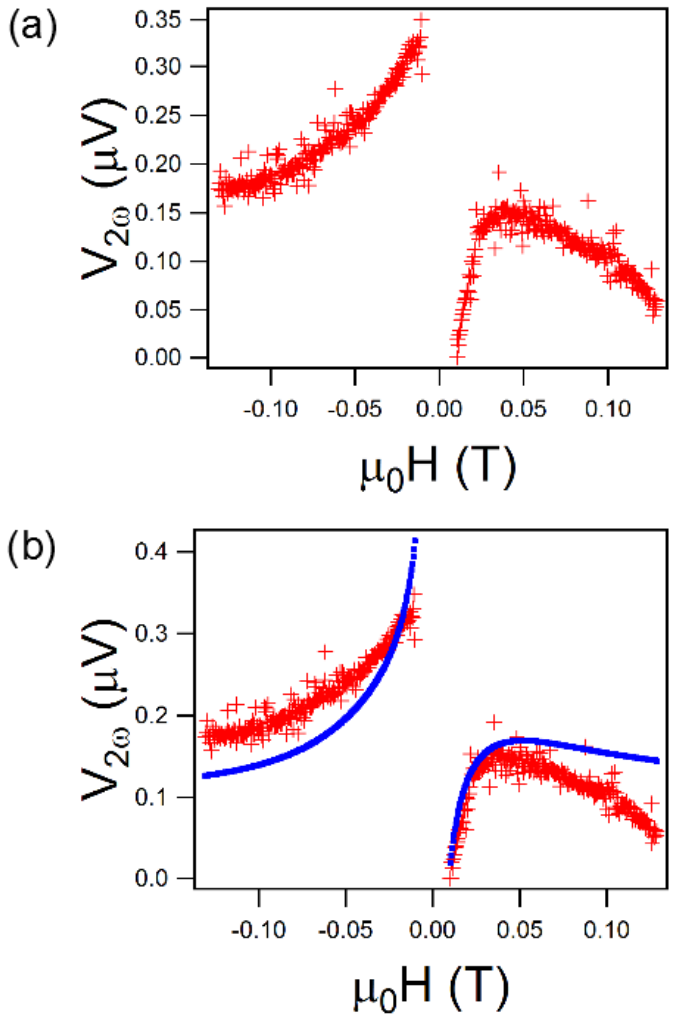

Fig. 3.7. (a) Our full measured second harmonic Hall signal as a function of applied magnetic field perpendicular to the current direction. The divergence near zero field results from the out-of-plane torque competing against the applied field, while the non-monotonic behavior in the positive field regime results from moving spin polarizations as the magnet pulls the source layer magnetization. (b) A fit to this data using only our primary model, with no other signals. Although the two have somewhat similar form, it is clear that our model is not quite the full picture.

It is now important to address the results observed from our control samples. If we observe parasitic signals in our control samples, it may be that those same parasitic signals will contribute to our primary measurement.

Additionally, these control samples allow us to further confirm spin current as the source of our primary signal by eliminating any single-layer parasitic signal as a possible source. As discussed earlier in this chapter, we have produced two relevant control samples, each lacking one of the two magnetic layers. We performed the same second-harmonic Hall measurement on each of these samples, with the applied magnetic field perpendicular to the current direction. The sample with no FeGd layer yields almost no field-dependent signal (Fig. 2(b)). This is as expected, because for our special geometry, the orientation of the CoFeB moment transverse to the current should prevent any signals due to spin Hall or Oersted torques and also any thermal signals due to the Nernst effect. Both of these mechanisms should depend only on the behavior of the CoFeB layer; therefore, this measurement allows us to confirm that these signals are indeed absent in our geometry. The second control sample, however, containing only the exchange biased FeGd layer and hafnium, shows a substantial parasitic signal, which, fortunately, has a different form from our primary signal. This, at least, confirms that the interesting behavior in our primary sample derives from an interaction between the two magnetic layers, as expected. We will now use our model for the various experimental artifacts that could contribute to our control samples, and examine the consequences to our primary sample. We have already examined such parasitic signals in the prior chapter, in the general case, and now need only apply the general model to our specific system. In doing this, we will not only explain the source of the parasitic signals in our control samples, but also

reconcile our final fits to our primary sample data.

3.4 Consequences of Oersted Torques for our Measurements

The geometry of our measurements limits the size of the CoFeB Oersted signal to be approximately zero, as the Oersted field is parallel to the CoFeB magnetization. A small misalignment could cause an Oersted signal to appear, but such a signal will fall off quickly with applied field and will therefore make no significant contribution to our data. The signal might be expected to contribute for very small applied field values, but we do not preserve the data very close to zero field, as discussed in the previous section.

The Oersted torque acting on the FeGd source layer is of more interest and concern than that acting on the CoFeB layer. We see the effects of such a torque in our FeGd control sample (see Fig. 3.8). However, for our primary sample, the applied current flowing through the layers above the FeGd is nearly equal to that flowing below the FeGd, and their Oersted fields largely cancel one another. Using the model outlined in section 2.6, Potential Parasitic Signals for Second Harmonic Hall Measurements with Two Magnetic Layers, we can estimate the size of the Oersted field Signals due to Oersted Torques, and, after we have measured the size of the planar Hall effect and exchange bias, as outlined earlier in this chapter, we may predict both the size and form of the Oersted torque planar Hall second

harmonic signal, and include it in our primary fit. We find the resulting Oersted field to be rather small. We also use our model to calculate the expected signal for the FeGd control sample, and find that it agrees fairly well with our measurements (see Fig. 3.8). The disagreement can be partially explained by a small anomalous Nernst signal in the FeGd layer, which proves too small to be important in our primary sample, as will be discussed in the next section. The remaining discrepancies may be explained by small disagreements between our model and the true sample, such as field misalignments or slight discrepancies in current values. The predicted signal for the Oersted field in our primary sample is quite small compared to our measured signal, and does not substantially contribute.

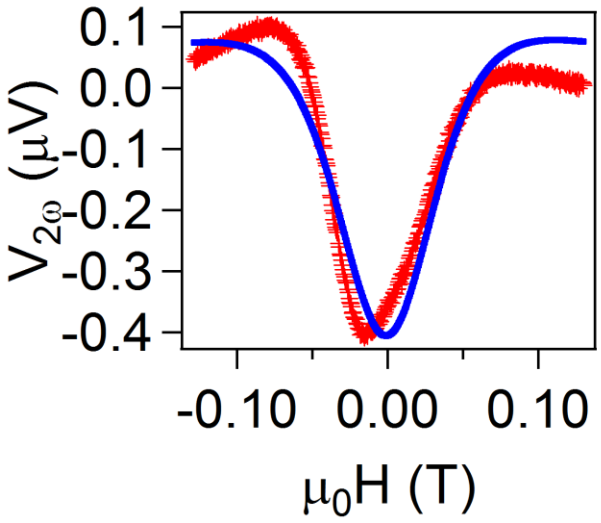

Fig. 3.8. Second harmonic Hall data for the IrMn/FeGd/Hf control sample (red markers), with calculated signal (blue line) using the calculated value for the Oersted field and the measured planar Hall resistance.

3.5 Consequences of the Anomalous Nernst Effect for our Measurements

We have chosen our geometry such that the anomalous Nernst signal due to our CoFeB source layer is nearly zero. However, we might nonetheless expect to see a very small constant term that changes sign when the CoFeB layer switches, due to experimental angular misalignments of up to a few degrees between the applied field and the current direction. We do, in fact, see a small anomalous Nernst effect in our CoFeB control sample (see Fig. 3.9), which further confirms the presence of a small misalignment. Although this signal is quite small, it bears some relevance to the analysis of our full sample data because it affects the data across our field range. Accordingly, we can account for this term by adding in a constant step function at zero applied magnetic field into the model we use for our final data. We will see that this term is fairly small (see Appendix B, Fit Procedures and Parameters for Second Harmonic Hall Measurements).

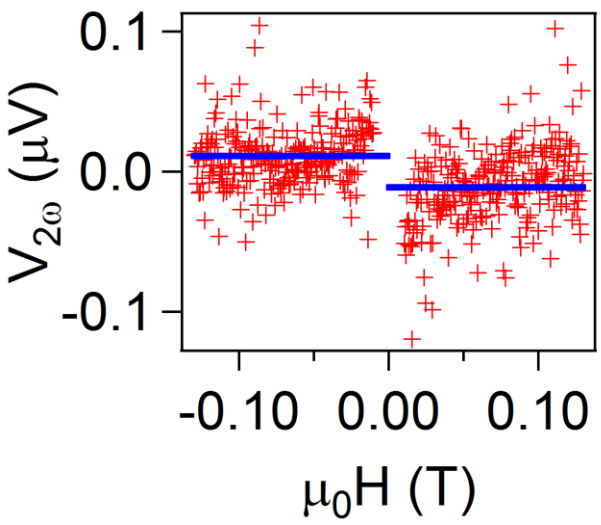

Fig. 3.9. Second harmonic Hall data for the IrMn/Hf/CoFeB/Hf control sample, with fit to a misalignment anomalous Nernst term.

Second, we may expect to see an anomalous Nernst signal generated in the FeGd layer, which varies smoothly as $V_{ANE} \mu \cos(j_{FeGd})$. Though this does prove to have small importance in our control sample measurement, a fit of the second harmonic data measured in the IrMn/FeGd control sample sets a bound of < 50 nV at 30 K for the V_{AHE} contribution. The size of the anomalous Nernst signal in the FeGd is small enough that it makes no meaningful contribution to the control samples, and so we do not need to include it in the model for our primary data.

3.6 Consequences of Exchange Coupling for our Measurements

We used Vibrating Sample Magnetometry to measure the coupling of the FeGd and CoFeB layers. By saturating the FeGd layer parallel to its exchange bias, because it has non-zero coercivity (see Fig. 3.10), we are able to sweep through the CoFeB switching while the FeGd layer remains parallel to the exchange bias. In this way, we can observe the CoFeB switching to ascertain whether the FeGd layer has substantial interlayer exchange coupling with the CoFeB sensor layer. A narrow field scan around zero applied magnetic field with the FeGd layer saturated is shown in Fig.3.10 (b). Were there any coupling between the FeGd and the CoFeB, the effective exchange field acting on the CoFeB would offset its switching from zero applied field, because the FeGd layer is saturated in the exchange bias direction. The switching is not appreciably offset, and from this data we conclude that the interlayer exchange coupling is very small (<10 Oe). We then used 10 Oe, the upper limit on the size of the exchange coupling effective field, to produce the model shown in Fig. 2.4, which indicates that this effect produces no notable signal outside of the small field range near zero applied field, which we have omitted from our data because the CoFeB undergoes a spatially non-uniform switching process in this field range.

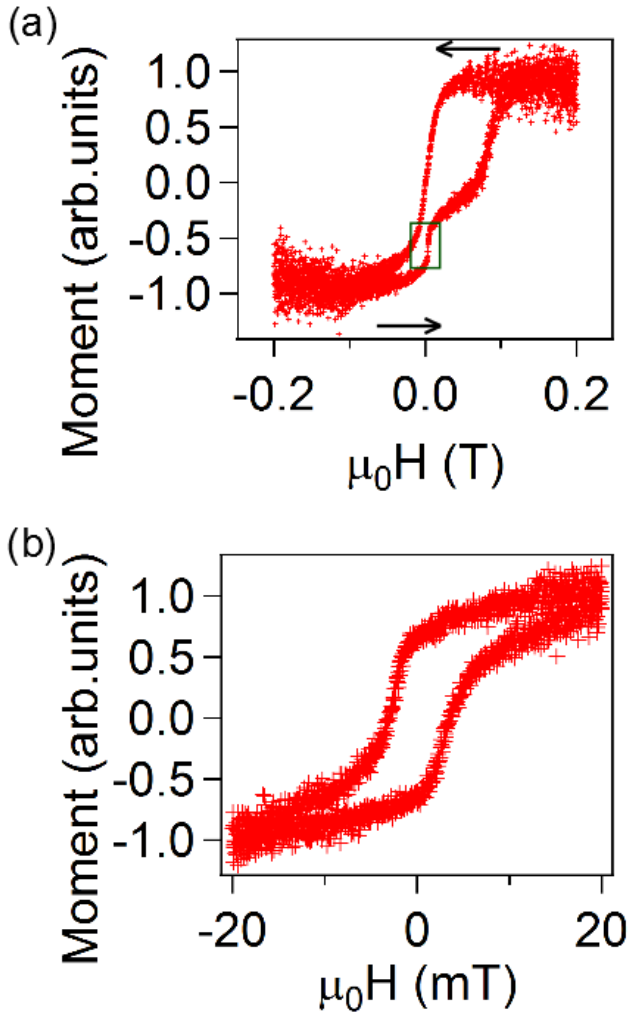

Fig. 3.10. (a) A depiction of the Vibrating Sample Magnetometry data for our full IrMn/FeGd/Hf/CoFeB/Hf stack, zoomed out. The green box indicates the location in the full hysteresis sweep at which the field may be swept in order to measure the exchange coupling between the magnetic layers. (b) A zoomed in scan showing only the component of the scan corresponding to the CoFeB switching, while the FeGd remains parallel to the exchange bias. The CoFeB switching is not visibly offset from zero applied field, which allows us to conclude that any exchange field between the two is small, <10 Oe.

3.7 Discussion

Figure 3.11 (a) shows the same data as is shown in Fig. 3.7 (a), the second harmonic Hall data taken for our primary sample with a fit to the theory of Taniguchi et al.[51] (blue line), as developed above, with our calculated small Oersted and Nernst signals included. With the inclusion of our parasitic signals, the fit conforms well to the measured data, while still deriving primarily from our reorientable spin orientation spin current.

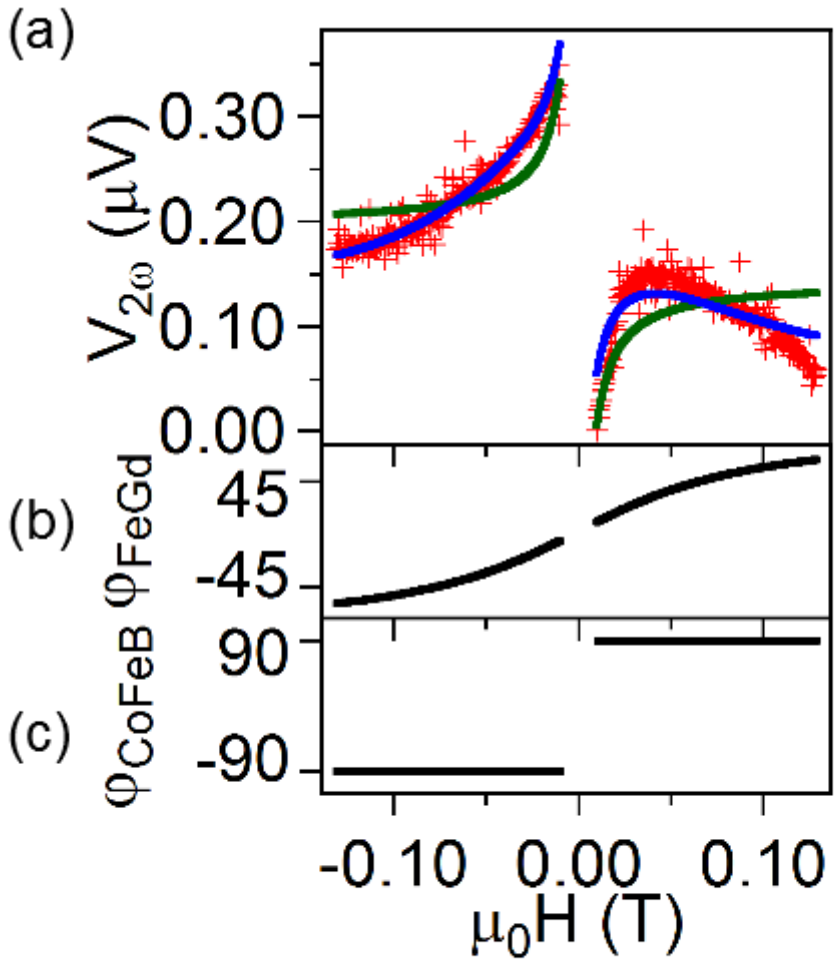

Fig. 3.11. (a) (a)The same data (red markers) as in Fig. 3.7 (a), with comparison to the model of Taniguchi et al.[51] (blue line), which assumes that $\vec{\sigma} \propto \left(\hat{y} \bullet \hat{m}_{\mathrm{FeGd}}\right)\hat{m}_{\mathrm{FeGd}}$, as well as a fit to a model which assumes that $\vec{\sigma}$ is constant (green line). (b,c) Dependence on the applied magnetic field for the magnetization angles j_{FeGd} and j_{CoFeB} within the fit.

Unlike the schematic shown in Table 2(c), the second-harmonic signal does not decrease symmetrically to zero at large positive and negative fields. This is

because the spin torque is not constant as a function of changing *H*, but changes as *H* reorients j_{FeGd}. To illustrate the necessity of taking into account the variation of the transverse spin current $\vec{\sigma}$ on the orientation of the FeGd moment, we have also performed a fit to the standard second harmonic Hall model, under the assumption that $\vec{\sigma}$ is a constant, independent of j_{FeGd} (green line), as laid out in section 2.1, Second Harmonic Hall Method for In-Plane Magnetic Layers. (This is somewhat artificial, since for the experimental geometry of Fig. 2(a) one should have $\vec{\sigma} = 0$ for conventional torques, as explained previously.) Any model assuming $\vec{\sigma}$ = constant is qualitatively inconsistent with the measurements, while taking into account the expected variation of $\vec{\sigma}$ with j_{FeGd} accounts well for the nonmonotonic dependence of the signal at positive fields. Finally, in order to further drive home the point that the Oersted signal in the FeGd layer does not contribute meaningfully to our final result, we show in Fig. 3.12 a comparison of our primary fit with and without the Oersted term included. The fit is not made appreciably worse by its removal.

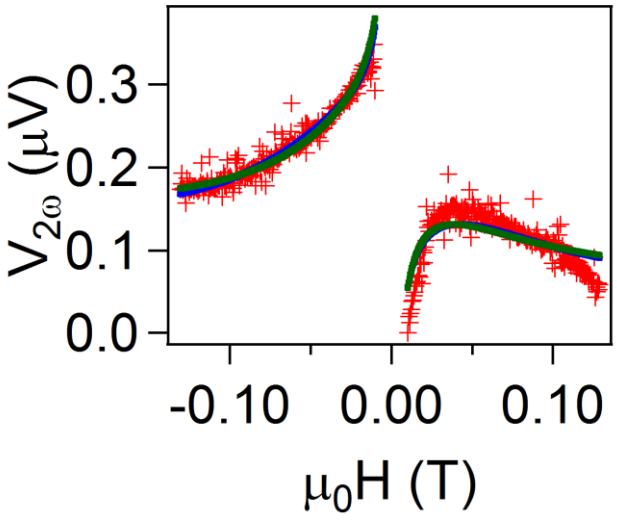

Fig 3.12. A comparison of our full fit (blue line) to a fit done neglecting a small, smooth background due to the Oersted field acting on the FeGd layer and producing a second harmonic signal via the planar Hall effect (green line).

We now wish to use our numerical model to extract the size of the spin current produced in the FeGd layer, and hence find a quantity analogous to a spin Hall angle for our ferromagnetic FeGd. We can characterize the strength of the out-of-plane field-like torque generated by the FeGd and acting on the CoFeB in terms of a spin-torque efficiency, $\chi_{FL,AHE}$, such that the spin-current-induced effective field acting on the CoFeB is $H_{FL}^{0} = \xi_{FL,AHE} \frac{\hbar}{2e\mu_0 M_s t_{FM}} J_e \sin(\varphi_{FeGd})$, where J_e is the applied charge current density in the FeGd, $\mu_0 M_s$ = 0.90 T is the saturation magnetization of the CoFeB layer based on VSM measurements of a IrMn/Hf/CoFeB/Hf control sample, and t_{FM} is the thickness of the ferromagnetic layer. Fitting the measured signal yields an estimated $\chi_{FL,AHE}$ of -0.9 ± 0.2%.

This value is a lower bound for the magnitude of the field-like spin-torque efficiency that can be generated by the FeGd because we do not account for less-than-perfect interface transparency. Many studies have in the past demonstrated that spin current losses at interfaces can be quite high. Moreover, based on past work from our research group and the Buhrman research group, we can conclude that there is a significant loss of spin current upon transmission through the hafnium, which has a spin diffusion length of approximately 1.5 nm [76,77], and therefore about half of the spin current may be expected to be lost to this effect.

3.8 Potential Anti-Damping Torques

An in-plane torque component may also be present in our samples, but the experimental geometry makes it more difficult to detect. Because our magnetic sensor layer lies in the plane of the sample, it is much easier to rotate the magnetization in-plane than to pull it out of plane. The signature of an in-plane torque in a second-harmonic Hall measurement is $1/|H_k|$, which is much less pronounced than the $1/|H|$ divergence for an out-of-plane torque, and is further obscured when the magnitude of the torque is field-dependent. Despite this, the measured anomalous Hall resistance of our CoFeB is much higher than its planar Hall resistance, and this effect may be expected to make the two signals nearly equal. However, because of the low sensitivity to in-plane torques, even small

miscalculations in our estimates of these values could render the anti-damping torque undetectable in actuality.

We have performed our fitting procedure with various values for the size of this anti-damping term, to determine the point at which the fitting becomes poor. This method gives a conservative upper bound of $\left|\mu_0 H_{AD}^0\right| \leq 46\ mT$ for I = 5.2 mA, (corresponding to an anti-damping spin torque efficiency ≤ 1.0 ± 0.3%). The limits on both positive and negative values of H_{AD}^0 are similar. However, this value does not necessarily reflect an upper bound on the maximum spin torque that can be produced by the FeGd layer, since this bound does not take into account attenuation of the spin current upon transmission through the Hf spacer layer or imperfect spin transmission at interfaces. That the damping-like torque is not much stronger than the field-like torque may be a consequence of the Hf/CoFeB interface. Previously we have observed that even though $\xi_{AD} >> \xi_{FL}$ in W/CoFeB devices that after the addition of a Hf spacer $x_{AD} < x_{FL}$ in W/Hf/CoFeB [77].

We note that Humphries et al. [78] have recently pointed out an alternative mechanism whereby an out-of-plane spin-orbit torque might be generated in a ferromagnet/spacer/ferromagnetic multilayer – a spin current generated by spin-orbit interactions with an in-plane spin polarization might precess in the exchange field of the fixed magnetic layer so that when the resulting spin current interacts with the sensor magnetic layer it can apply an out-of-plane anti-damping torque. We can tell that this mechanism is not dominant in our measurement because the

out-of-plane torque we measure is a field-like torque, not an anti-damping torque, based on the sign change we observe in the component of the second-harmonic Hall signal proportional to $1/|H|$ upon reversal of the CoFeB magnetization near zero field.

CHAPTER 4

ST-FMR AND FUTURE SPIN TORQUE DETECTION METHODS

It is valuable to consider additional techniques for measuring conventional spin currents, and their utility for the more complicated anomalous Hall spin currents. Widely used techniques include spin-torque ferromagnetic resonance (ST-FMR), the magneto-optic Kerr effect (MOKE), and spin pumping. These methods sometimes produce contradictory estimates for the spin Hall effect when applied to the same material, and some of these techniques are more sensitive to exotic torques than others. It is therefore interesting to apply several different experimental techniques to generate a more complete picture of the underlying physics. Additionally, the various methods use different means of detecting spin torques, and so are subject to different parasitic signals and potential difficulties. Thus, confirming our measurements using additional techniques will help establish more concretely the truth of our claims. Like the second harmonic Hall method, however, these methods are each complicated when applied to two-ferromagnet systems.

When measuring anomalous Hall spin torques using MOKE, we risk sensitivity to the magnetic state of the generating ferromagnetic layer as well as that of the sensor ferromagnetic layer. It is thus a design challenge to engineer the experiment to properly distinguish between the two signal sources. With correct

choices of materials, however, it would likely be possible to use MOKE to probe the effect. We have not yet pursued this measurement avenue, but it holds substantial promise for the future.

Spin pumping is complicated by the presence of a second ferromagnetic layer. If the two layers have resonance frequencies close to one another, both magnets might pump spin currents. Additionally, coupling between the two magnetic layers could couple the resonances of the two layers together, leading to complicated behavior. However, if the two layers are appropriately decoupled, and their resonance frequencies are sufficiently far apart, then by tuning to the resonant frequency of the selected spin pumping ferromagnet, it is possible to ensure that the dominant source of spin current is from the chosen magnetic layer. In this way, we could measure the inverse of the anomalous Hall spin current – the anomalous Hall analogue to the inverse spin Hall effect. The inverse spin Hall effect in ferromagnets has been measured by several groups, as mentioned earlier in this document[42-47].

However, none of these techniques especially concern us in this document, except as potential future research directions. Instead, we wish to focus on ST-FMR, and its promise for measuring anomalous Hall spin currents.

4.1 DC-Biased ST-FMR

In this section, I will discuss a method of measuring the anomalous Hall spin current using ST-FMR put forward by Iihama et al.[79]. Using an exchange bias to control the direction of the generating anomalous Hall layer magnetization proves difficult during ST-FMR measurements, due to the relatively large magnetic fields required to hit the magnet's resonance. Such large fields will reorient the source layer magnetization away from the exchange bias direction, and, moreover, will cause the orientation to change as the applied field is being swept through resonance. It therefore becomes difficult to observe the reorientation of the spin polarization. However, if the generating magnetic layer is not controlled via an exchange bias, both layers will saturate in the same direction, and the spin polarization defined by the magnetization of the source layer will lie parallel to the sensor layer magnetization. Then, the spin torque exerted on the sensor layer by that spin current will fall to zero, as can be seen by a quick examination of the LLGS equation,

$$\frac{d\vec{\boldsymbol{m}}}{dt} = -\gamma \vec{\boldsymbol{m}} \times \vec{\boldsymbol{H}}_{tot} + \alpha \vec{\boldsymbol{m}} \times \frac{d\vec{\boldsymbol{m}}}{dt} + \gamma H_{FL} \vec{\boldsymbol{m}} \times \hat{\boldsymbol{\sigma}} + \gamma H_{AD} \vec{\boldsymbol{m}} \times \left(\hat{\boldsymbol{\sigma}} \times \vec{\boldsymbol{m}} \right). \tag{4.1}$$

Fortunately, Oersted torques still influence the sensor magnetic layer as usual, and will drive the magnetic sensor layer into resonance in the absence of a spin torque. We can still see a resonance, albeit one not driven by spin torque, and it turns out this is sufficient to make the measurement useful.

Because ST-FMR is not the primary concern of this thesis, and additionally, because other members of my research group (Alex Mellnik in particular, see his thesis[80]) have covered the technique of DC-biased ST-FMR in substantial detail, I will only briefly describe the premise of ST-FMR measurements, before outlining the modifications needed to detect spin currents from an anomalous Hall spin source layer.

The resistance of a magnetic layer has a component that changes depending on the orientation of the magnetization of the layer. This effect is known as anisotropic magnetoresistance (AMR), and can be expressed as $R = R_0 + R_{AMR}\cos^2(\varphi)$, for some AMR resistance R_{AMR}, and where ϕ, as usual, designates the angle between the current direction and the magnetization of the magnetic layer. When torques generated from exterior sources cause the magnetization of the sensor layer to rotate away from its equilibrium position, the magnetization will precess at a frequency dependent on the magnetic properties of the sensor layer and the strength of the applied magnetic field. As the magnetization moves, the resistance of the layer varies via the AMR with a frequency equal to the frequency of precession. A material with RF time-oscillating resistance subject to an RF time-oscillating current will produce a DC mixing voltage from the interaction between the two, whose size will only be significant when the two frequencies approach resonance. Because the precession frequency depends on the strength of the applied magnetic field, it is possible by sweeping an applied magnetic field to move the precession frequency through the resonance

condition afforded by the applied current frequency, and observe the resulting lineshape. Such measurements can be used to extract the strength of the torques causing the precession, if the size of the AMR and the magnetic properties of the sensor layer are known.

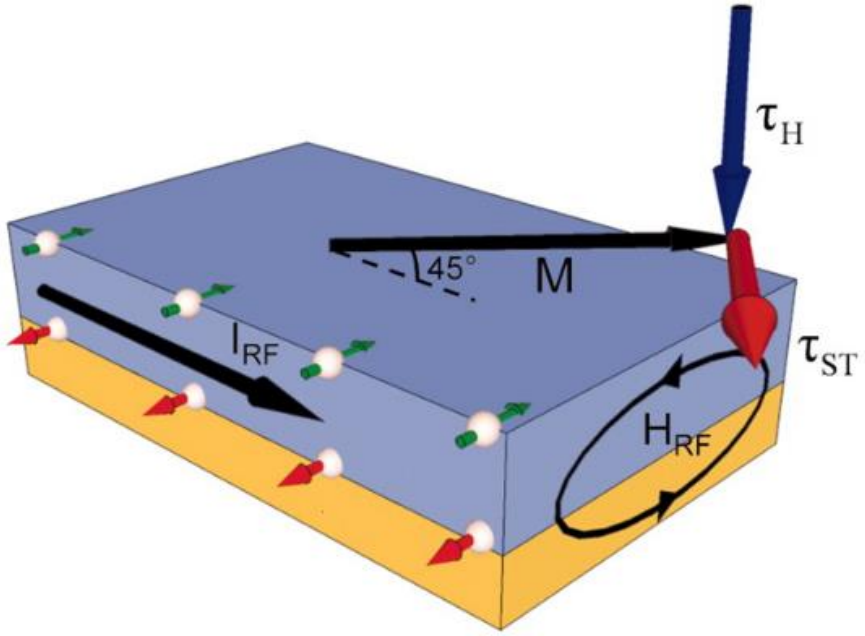

Fig. 4.1[57]. An illustration of the mechanism by which ST-FMR functions Torques kick the magnetization of the sensor layer away from its equilibrium position, creating AMR, which mixes with the applied RF current to generate a DC mixing voltage. The field-like torques, primarily the Oersted torque are denoted as τ_H and the anti-damping spin torques are designated as τ_{ST}.

For reasons that are discussed in detail within Alex Mellnik's thesis[80], and so will not be discussed here, the lineshape of the resonance consists of an asymmetric Lorentzian contribution due to traditional out-of-plane torques, such as the field-like spin Hall torque and the Oersted torque, and a symmetric Lorentzian

contribution due to traditional in-plane torques, such as the anti-damping torque, as

$$V_{Mix} = S\frac{\Delta H^2}{\left(H - H_0\right)^2 + \Delta H^2} + A\frac{\Delta H\left(H - H_0\right)}{\left(H - H_0\right)^2 + \Delta H^2} \ , \tag{3.2}$$

in which S is the size of the symmetric component, A is the size of the anti-symmetric component, ΔH is the linewidth, and H_0 is the resonance field. By fitting to the lineshape, it is then possible to extract the size of S and A, which are related to the size of the relevant torques. It is possible to extract other pieces of information from this fit, as well. In particular, the linewidth of the resonance may be used to determine the size of the damping, α in the LLGS equation above, of the magnetic sensor layer. Most importantly to our applications, however, it is possible to effectively modify this damping using a DC spin torque.

We may simultaneously apply a DC charge current and an RF charge current to our device. Although the RF spin current created will exert no torque and will not drive the sensor layer into resonance, the ordinary Oersted torque will still generate precession and create a resonance. However, although the DC spin current will not exert an ordinary torque on the sensor layer, it will interact with the sensor layer magnetization via second-order effects. The spin polarization of the induced spin current lies parallel to the equilibrium axis of the sensor layer magnetization ($\vec{\sigma} \parallel \vec{m}_0$), about which the magnetization precesses. However, the spin polarization is perpendicular to the component of the magnetization transverse to its equilibrium – that is, the spin torque can interact with the component of the magnetization that is precessing. The result of this torque is to either encourage or

discourage the precession, either increasing or decreasing the effective damping depending on the sign of the torque. This result is derived in some detail in the supplement to Iihama's paper[79], and so here we will simply quote the end result for the linewidth,

$$\Delta H = \Delta \mathrm{H}_0 + \frac{\omega}{\gamma}\left(\alpha - \frac{\hbar}{2e}\frac{\xi_{AHE} J_c \cos(\varphi)}{\left(H + \frac{M_{eff}}{2}\right) M_s d}\right) \tag{3.3}$$

The effective damping, and hence the linewidth of the resonance, is modified by an amount proportional to the applied DC spin current. Hence, by performing ST-FMR with varied values of applied DC-bias current, the linear change in effective damping can be used to extract the size of the DC spin current, even when the source magnetic layer is collinear with the magnetic sensor layer.

It is important to note that for measurements with two ferromagnetic layers, each layer will show a resonance due to Oersted torques, and so it is important to distinguish the two resonances from one another. As before, we will need to separate the two layers with a spacer so that they do not couple. Then, by making the two layers with sufficiently different saturation magnetizations, it is easy to see from the Kittel equation, $f = \frac{\gamma}{2\pi}\sqrt{H\left(H+M\right)}$ for the frequency of resonance, that for a given frequency, the resonant field can be made far enough apart to be easily distinguishable. By measuring the saturation magnetizations of the two layers, it is then possible to identify which resonance belongs to which layer. Ideally, we may

make one of the layers' magnetizations large or small enough that our measurement is only sensitive to our sensor layer.

In the following section, I will detail some ongoing measurements we have performed and are performing using this technique to detect spin currents generated by the anomalous Hall effect.

4.2 Materials and Methods

Alloys of Cobalt and rare earth materials offer a promising avenue for generation of anomalous Hall spin currents because they can be grown to be out of plane in the correct compositions, and for the correct choice of materials[81,82], and may have large spin Hall angles due to the presence of strong spin orbit coupling in the rare earth material. We elected to try the anomalous Hall spin current DC-biased ST-FMR technique on an alloy of cobalt and holmium, and additionally on permalloy, in order to examine the effectiveness of the technique, and to determine the size of the anomalous Hall spin currents in the two materials.

In order to probe these effects, we co-sputtered cobalt and holmium to produce a CoHo alloy of the desired proportions. Then, we sputtered a hafnium spacer layer in order to magnetically isolate the two magnetic layers, followed by either a cobalt, permalloy, or CoFeB sensor layer, producing one sample with each sensor. By preparing multiple samples using different sensor layers, we can repeat

the measurement with several sensor layer materials. If the spin Hall angle is the same in the two samples, irrespective of which sensor layer is used, we can better ensure that no complicated interplay between the two layers is responsible for the spin torques. We repeated the same sputtering process using permalloy as the spin source layer, and additionally produced samples with permalloy as the active layer, copper as the spacer layer, and CoFeB as the sensor layer.

We then patterned the devices using the same processes outlined for our second harmonic Hall measurements. ST-FMR bar devices are shown in the schematic in Fig. 4.2. This work is ongoing, and at the moment, we have measured only the samples with CoHo as the source layer and CoFeB as the sensor layer. We performed DC-biased spin torque FMR, as outlined in the prior section, by applying an RF current mixed with a DC bias current, and detecting the DC mixing voltage induced across the device. The results of this measurement are outlined in the following section.

4.3 CoHo ST-FMR Measurements

We apply an RF frequency current with total power of 20 dBm to our ST-FMR devices via a bias tee, as can be seen in Fig. 4.2, which shows a schematic diagram of our DC-biased ST-FMR measurements.

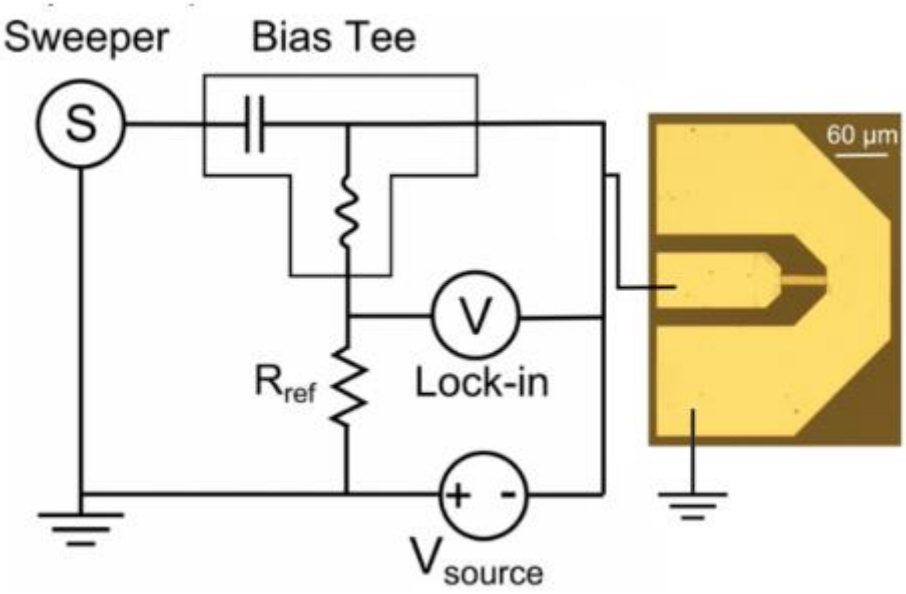

Fig. 4.2. A schematic diagram of our ST-FMR setup, with DC current applied. An image of an example ST-FMR device can be seen in the schematic.

The RF current causes resonance via Oersted torques, and the DC current creates a DC spin torque that modifies the linewidth of the resonance. We then apply a magnetic field in-plane at an angle of 45° with respect to the current direction, and sweep the strength of the magnetic field through the resonance condition, both for positive and negative field values. We repeat these measurements for a wide variety of DC bias current sizes (both positive and negative), and RF current frequencies. Each scan is then fit to a sum of anti-symmetric and symmetric Lorentzians, though, as expected, the anti-symmetric Lorentzian proves to be the dominant feature. One such example scan, with fit, is shown in Fig. 4.3.

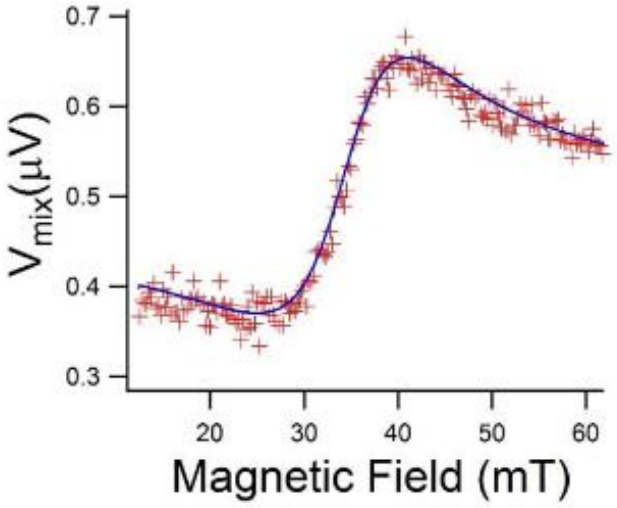

Fig. 4.3. The mixing voltage (red) as the magnetic field is swept through resonance, accompanied by a fit (blue) to a sum of an anti-symmetric and a symmetric Lorentzian centered about the resonance magnetic field.

Because we have a variety of frequencies and DC-bias currents, we may increase the accuracy of our method by conducting fits to both frequency and DC-bias current. The frequency dependence of the linewidth is not quite linear, because the resonance field and the frequency are related via the Kittel equation. For $M_s \gg H$, however, as is true in our samples, it is nearly linear, and so a linear fit to frequency may be taken. We therefore first fit to frequency, and extract the slope of the frequency dependence to obtain the effective damping. An example of this data, with the corresponding linear fit, is depicted in Fig. 4.4 (a). We then use a linear fit to the effective damping, shown in Fig. 4.4 (b) to extract the damping increase due to the applied DC spin torque. If the M_s is comparable to H, or extreme precision is desired, the linear fit to the DC current may be taken first, and

followed by a more precise non-linear fit to the formula in Eq. 3.3.

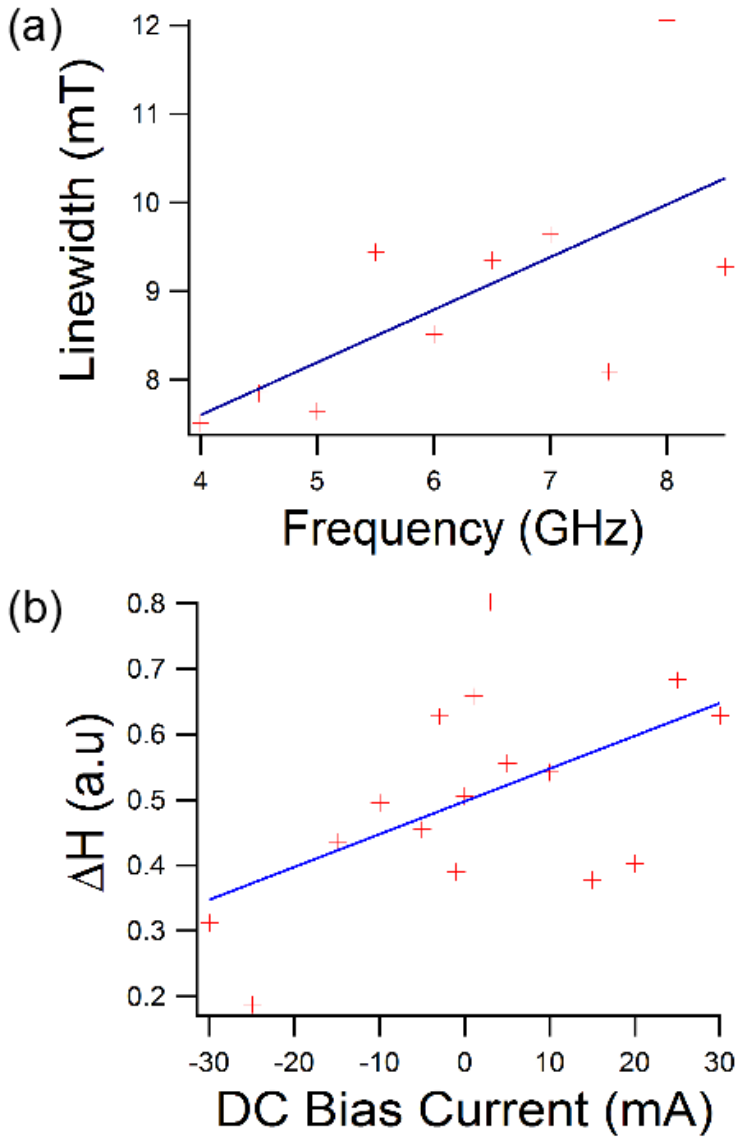

Fig. 4.4. (a) The Lorentzian linewidth extracted from the ST-FMR fit at I_{DC} = 0 mA, with a linear fit used to extract the effective damping. (b) The frequency dependent linewidth for various frequency values, accompanied by the linear fit used to extract the change in the damping due to the DC spin torque.

Before we can extract the spin torque efficiency from this data, we must ascertain the values of the effective magnetization, M_{eff}, and the saturation magnetization, M_s. M_{eff} may be extracted from the resonance lineshape, or from the Kittel formula, and M_s is measured via VSM. The two are generally very nearly the same, and are each estimated to be around 0.4T. With these values, the known constants, the resonance field, the frequency, and the thickness of the magnetic sensor layer, we can extract the value of the spin torque efficiency.

Measurements for this work are ongoing, but our preliminary estimates set a lower bound on the spin torque efficiency of about ~3.5%. The actual intrinsic spin torque efficiency in the CoHo could be quite a lot higher, due to spin current losses at the interface and due to the hafnium spacer layer. Additional lower-noise measurements will be possible in the future using a permalloy sensor layer, which exhibits substantially larger AMR, and may lead to more accurate estimates of the spin torque efficiency. Angular dependence measurements on these CoHo samples and permalloy samples are ongoing to confirm the anomalous Hall spin torque angular dependence.

4.4 Conclusions and Future Outlook

We have successfully used a second harmonic Hall system to measure spin torque generated with controllable spin polarization via the anomalous Hall effect,

demonstrating the ability to reorient that spin polarization through the application of a magnetic field, and produce field-like torques with controllable effective field direction. This allowed us to generate torque in cases in which none would exist for standard spin Hall torques. Additionally, we have tentatively confirmed the existence of anti-damping torques generated from the anomalous Hall effect via DC-biased ST-FMR.

In future, the two techniques detailed in this thesis may certainly be performed with better accuracy, lower noise, and more optimal spin materials. In this way, it will be possible to confirm the results detailed in this thesis, as well as to find materials with higher spin torque efficiencies and improve our capabilities for torque generation.

Beyond repetition and improvement of the two techniques at hand, there is yet more room for innovation and design of new experimental techniques to test the full extent of the versatility of anomalous Hall effect spin currents. In the introduction to this document, we specified that we wish to create out-of-plane anti-damping torques, but this thesis has not shown such a creation. It has merely shown that the spin polarization of spin currents generated by the anomalous Hall effect may be controlled. Although this suggests that it should be possible to generate out of plane anti-damping torques, additional experimentation is needed to prove this conjecture. Such experiments, however, require the creation of anomalous Hall source layers with magnetizations tilted significantly out of the plane of the sample, while still maintaining an in-plane component necessary to

generate upward travelling spin current, which has proven to be a challenge for material production. One needs to engineer a magnetic layer that is partially out of plane, and partially in-plane, and yet also has a large spin Hall angle.

I note here that we have attempted to engineer such samples on a few occasions, primarily with alloys of cobalt and rare earth elements, with limited success, as the heat of sample processing seems to destroy the perpendicular magnetic anisotropy naturally present in the rare earth-cobalt alloy. This work is thus ongoing.

One more obstacle, however, presents itself before anomalous Hall spin currents can truly be said to be practical for magnetic switching. We will need to show that applied anomalous Hall spin currents are capable of generating sufficiently strong out-of-plane anti-damping torques to switch nanomagnets. For this purpose, it is useful to create a sample consisting of two out-of-plane layers, one thin sensor layer, and one anomalous Hall source layer. The source layer may be tilted in-plane, either naturally, or induced into that direction by an exchange bias or in-plane magnetic field. The sensor layer may then be switched by applying a sufficiently strong current pulse through the source layer. This goal, though incredibly exciting, is quite difficult to achieve without first taking smaller steps in our comprehension of anomalous Hall spin currents, which will be achievable naturally by continuing the research outlined in this thesis.

APPENDIX A

Detailed Description of Fabrication Processes

Our materials are grown on cleaned sapphire substrates in a Kurt J. Lesker sputtering system, using 3” TORUS guns (1” for Holmium) at base pressure ~1E-9 Torr. The substrates are rotated during deposition, which is conducted at pressures ranging from 2 mTorr (most of our materials) to 4 mTorr (permalloy) and 5 mTorr (CoHo alloys), and powers ranging from 20 W (most of our materials), up to 135 W (for our highest Co-composition CoHo alloys). The deposition rates for the guns are calibrated by depositing the relevant material onto silicon wafers patterned with large features in Shipley 1805 photoresist, following the process outlined below for S-1805’s use with our primary samples. The calibration substrates are then sonicated in acetone for 30 seconds to lift off the photoresist, and the thickness is characterized using profilometry.

Once our materials are grown, we apply photoresist to our samples according to the following procedure:

1. Apply LOR-3A in the Class 2 Resist room at the CNF and spin the resist according to the parameters: 1 minute; 1000 RPM/s acceleration; and 3000 RPM speed.
2. Bake for 5 minutes at 180C.
3. Apply S-1805 photoresist in the photoresist room, and spin according to the parameters: 1 minute; 1000 RPM/s acceleration; and 3000 RPM speed.

4. Bake for 1:15 at 115C.

Subsequently, we pattern the device by exposing it through a mask on the CNF 5x g-line stepper, using the etch layer of the die shown in Fig. 3.2 in the main document to define Hall bars, with the process as follows:

1. Expose the sample according to the pattern for 0.25 seconds.
2. Develop the sample in MIF-726 for 1 minute.
3. Clean the sample with DI water.

We then use an ion milling system belonging to the Buhrman group to etch away the material other than the desired bar structures and alignment marks, and remove the photoresist by leaving the samples overnight in 180C 1165. After the 1165 is allowed to cool, the samples are sonicated for 30 seconds, still in 1165. They are subsequently cleaned with water and dried with pressurized air.

The samples are cleaned with acetone and isopropyl alcohol and dried before the next step of patterning. Afterward, the above photolithography process is repeated (steps 1-4, and steps 1-3, outlined above) using a photomask designed for top leads, and using an aligned exposure on the 5x stepper. Subsequently, the CNF AJA sputter deposition system is used to deposit 3 nm of Titanium followed by 180 nanometers of platinum in order to define contact pads. The samples are then placed once again into 180C 1165 and left overnight. After the 1165 is allowed to cool, the samples are again sonicated for 30 seconds.

Our photomasks are designed in L-Edit and created using the Heidelberg

Mask Writer DWL2000.

For samples used for the second harmonic Hall project, but not for ST-FMR, an annealing process is necessary to set the exchange bias direction in the IrMn.

The samples are taken and rotated such that their horizontal direction is aligned with an applied magnetic field within the magnetic sample holder for the CCMR Lindberg vacuum furnace. That sample holder is then placed into the Lindberg vacuum furnace and heated to a nominal temperature of 420K for one hour, after which the furnace is cooled until the sample can be removed. This process effectively sets an exchange bias direction. At this point, the samples are ready for measurement.

APPENDIX B

Fit Procedures and Parameters for Second Harmonic Hall Measurements

We determined the following fixed parameters by independent measurements:

In the CoFeB layer:

$IR_{PHE} = 0.17 \pm 0.02$ mV was determined by measuring the Hall voltage using a lock-in amplifier while rotating the direction of an in-plane magnetic field applied to the CoFeB control sample, maintaining the same current through the CoFeB layer as in the primary sample.

In the FeGd layer:

$IR_{PHE}\mu_0 H_{Oe} = -4 \pm 1$ nV T was calculated, and separately confirmed using the FeGd control, as outlined above.

$\mu_0 H_{ex}$ = 0.070 ± 0.001 T, measured with a linear field first harmonic measurement with the field perpendicular to the exchange bias.

After accounting for the signal due to the Oersted field acting on the FeGd layer as discussed above, we fit the measured data to Eq. (S6) (with $H_{AD}^{0} = 0$) using three adjustable parameters plus an overall offset voltage. The fit equation is as follows.

$$V^{2f} = -IR_{\mathrm{PHE}} \frac{H_{FL}^{0} \sin\left(2\varphi_{FeGd}\right)}{4H} + V_{Offset} + V_{ANE,Misalignment}\,\mathrm{sgn(H)} + IR_{\mathrm{PHE}} \cos\left(2\varphi_{FeGd}\right) \frac{H_{Oe}\cos(\varphi_{FeGd})}{2\sqrt{H^2 + H_{EB}^2}} \ ,$$

with $j_{FeGd} \approx j^{0}_{FeGd} + \tan^{-1}(H / H_{ex})$.

Using this fit, we determine the following values.

H^{0}_{FL} = 0.14 ± 0.02 mT for *I* = 5.2 mA.

j^{0}_{FeGd} = 3.1° ± 0.2°

$V_{ANE,Misalignment}$ = 43 ± 2 nV

REFERENCES

[1] A. M. Caulfield, J. Coburn, T. I. Mollov, A. De, A. Akel, J. He, A. Jagatheesan, R. K. Gupta, A. Snavely, and S. Swanson, *Understanding the Impact of Emerging Non-Volatile Memories on High-Performance, IO-Intensive Computing,* Proc. SC 2010 (2010).

[2] I. Ennen, D. Kappe, T. Rempel, C. Glenske, and A. Hütten, *Giant Magnetoresistance: Basic Concepts, Microstructure, Magnetic Interactions and Applications*, Sensors (Basel) **16**, 904 (2016).

[3] B.H. Miller and E. D. Dahlberg, *Use of the anisotropic magnetoresistance to measure exchange anisotropy in Co/CoO bilayers*, Appl. Phys. Lett. **69**, 3932 (1996).

[4] M. N Baibich, J. M. Broto, A. Fert, F. Nguyen Van Dau, F. Petroff, P. Etienne, G. Creuzet, A. Friederich, J. Chazelas, *Giant Magnetoresistance of (001)Fe/(001)Cr Magnetic Superlattices*, Phys. Rev. Lett. **61**, 2472 (1988)..

[5] G. Binasch, P. Grünberg, F. Saurenbach, and W. Zinn, *Enhanced magnetoresistance in layered magnetic structures with antiferromagnetic interlayer exchange*, Phys. Rev. B **39**, 4828 (1989).

[6] R. Meservey and P.M. Tedrow, *Spin Polarization of Tunneling Electrons from Films of Fe, Co, Ni, and Gd*, Solid State Commun. **11**, 333 (1972).

[7] M. Julliere, *Tunneling between ferromagnetic films*, Phys. Lett. A **54**, 225 (1975).

[8] L. M. Loong, X. Qiu, Z. P. Neo, P. Deorani, Y. Wu, C. S. Bhatia, M. Saeys, and H. Yang, *Strain-enhanced tunneling magnetoresistance in MgO magnetic tunnel junctions*, Sci Rep. **4**, 6505 (2014).

[9] L. Berger, *Low-field magnetoresistance and domain drag in ferromagnets,* J. Appl. Phys. **49**, 2156 (1978).

[10] L. Berger, *Domain drag effect in the presence of variable magnetic field or variable transport current*, J. Appl. Phys. **50**, 2137 (1979).

[11] J. C. Slonczewski, *Conductance and exchange coupling of two ferromagnets separated by a tunneling barrier*, Phys. Rev. B **39**, 6995 (1989).

[12] J. C. Slonczewski, *Current-driven excitation of magnetic multilayers*, J. Magn. Magn. Mater. **159**, L1 (1996).

[13] L. Berger, *Emission of spin waves by a magnetic multilayer traversed by a current*, Phys. Rev. B. **54**, 9353 (1996).

[14] T. L. Gilbert, *A phenomenological theory of damping in ferromagnetic materials*, IEEE Trans. Magn. **40**, 3443 (2004).

[15] Y. Huai,F. Albert, P. Nguyen, M. Pakala, and T. Valet, *Observation of spin-transfer switching in deep submicron-sized and low-resistance magnetic tunnel junctions*, Appl. Phys. Lett. **84**, 3118 (2004).

[16] J. Katine, F. Albert, R. Buhrman, E. Myers, and D. C. Ralph, *Current-Driven Magnetization Reversal and Spin-Wave Excitations in Co /Cu /Co Pillar.,* Phys. Rev. Lett. **84**, 3149 (2000).

[17] G. D. Fuchs, N. C. Emley, I. N. Krivorotov, P. M. Braganca, E. M. Ryan, S. I. Kiselev, J. C. Sankey, D. C. Ralph, and R. A. Buhrman, *Spin-transfer effects in nanoscale magnetic tunnel junctions*, Appl. Phys. Lett. **85**, 1205 (2004).
[18]M. I. D'Yakonov and V. I. Perel, *Possibility of Orienting Electron Spins with Current*, ZhETF Pis. Red. **13**, 657 (1971).
[19] Y. K. Kato,, R. C. Myers, A. C. Gossard, and D. D. Awschalom, *Observation of the Spin Hall Effect in Semiconductors*, Science **306**, 1910 (2004).
[20] J. Wunderlich, B. Kaestner, J. Sinova, and T. Jungwirth, *Experimental Observation of the Spin-Hall Effect in a Two-Dimensional Spin-Orbit Coupled Semiconductor System*, Phys. Rev. Lett. **94**, 047204 (2005).
[21] J. Sinova, D. Culcer, Q. Niu, N. A. Sinitsyn, T. Jungwirth, and A. H. MacDonald, *Universal Intrinsic Spin Hall Effect,* Phys. Rev. Lett. **92**, 126603 (2004).
[22] S. Murakami, N. Nagaosa, and S. C. Zhang, *Dissipationless Quantum Spin Current at Room Temperature*, Science **301**, 1348 (2003).
[23]M. V. Berry, *Quantal phase factors accompanying adiabatic changes*, Proc. R. Soc. London, Ser. A **392**, 45 (1984).
[24] M. Gradhand, D. V. Fedorov, F. Pientka, P. Zahn, I. Mertig, and B. L. Gyorffy, *First-principle calculations of the Berry curvature of Bloch states for charge and spin transport of electrons*, J. Phys. Condens. Matter **24**, 213202 (2012).
[25] M. I. Dyakonov and V. I. Perel, *Current-induced spin orientation of electrons in semiconductors*, Phys. Lett. **A35**, 459 (1971).
[26] S. Zhang, *Spin Hall Effect in the Presence of Spin Diffusion*, Phys. Rev. Lett. **85**, 393 (2000).
[27] J. E. Hirsch, *Spin Hall Effect in the Presence of Spin Diffusion*, Phys. Rev. Lett. **83**, 1834 (1999).
[28] G. Vignale, *Ten Years of the Spin Hall Effect*, J. Supercond. Nov. Magn. **23**, 3 (2010).
[29] A. R. Mellnik, J. S. Lee, A. Richardella, J. L. Grab, P. J. Mintun, H. M. Fischer, A. Vaezi, A. Manchon, E. –A. Kim, N. Samarth, and D. C. Ralph, *Spin-transfer torque generated by a topological insulator*, Nature **511**, 449 (2014).
[30] Y. Fan et al., *Magnetisation switching through giant spin-orbit torque in a magnetically doped topological insulator heterostructure*. Nature Mater. **13**, 699 (2014).
[31] N. H. D. Khang, Y. Ueda, and P. N Hai, *A conductive topological insulator with colossal spin Hall effect for ultra-low power spin-orbit-torque switching*, arXiv:1709.07684 (2017).
[32] D. MacNeill, G. M. Stiehl, M. H. D. Guimaraes, R. A. Buhrman, J. Park, and D. C. Ralph, *Control of spin–orbit torques through crystal symmetry in WTe2/ferromagnet bilayers*, Nat. Phys. **13**, 300 (2017).
[33] T. A. Gosavi, S. Manipatruni, S. V. Aradhya, G. E. Rowlands, D. Nikonov, I. A. Young, S. A. Bhave, *Experimental Demonstration of Efficient Spin-Orbit Torque*

Switching of an MTJ with sub-100 ns Pulses, IEEE Trans. Magn. **53**, 3400607 (2017).
[34] S. Shi, Y. Ou, S. V. Aradhya, D. C. Ralph, and R. A. Buhrman, *Fast Low-Current Spin-Orbit-Torque Switching of Magnetic Tunnel Junctions through Atomic Modifications of the Free-Layer Interfaces*, Phys. Rev. Appl. **9**, 011002 (2018).
[35] S. O. Valenzuela and M. Tinkham, *Direct electronic measurement of the spin Hall effect*, Nature **442**, 176 (2006).
[36] E. Saitoh, M. Ueda, H. Miyajima, and G. Tatara, *Conversion of spin current into charge current at room temperature: Inverse spin-Hall effect*, Appl. Phys. Lett. **88**, 182509 (2006).
[37] E. Hall, *On the "rotational coefficient" in nickel and cobalt,* Phil. Mag. **12**, 157 (1881).
[38] E. Pugh, *Hall Effect and the Magnetic Properties of Some Ferromagnetic Materials*, Phys. Rev. **36**, 1503 (1930).
[39] R. Karplus and J. Luttinger, *Hall Effect in Ferromagnetics*, Phys. Rev. **95**, 1154 (1954).
[40] J. Smit, *The spontaneous hall effect in ferromagnetics I*, Physica **21**, 877 (1955).
[41] L. Berger, *Influence of spin-orbit interaction on the transport processes in ferromagnetic nickel alloys, in the presence of a degeneracy of the 3d band*, Physica **30**, 1141 (1964).
[42] B. F. Miao, S. Y. Huang, D. Qu, and C. L. Chien, *Inverse Spin Hall Effect in a Ferromagnetic Metal*, Phys. Rev. Lett. **111**, 066602 (2013).
[43] T. Seki, K. Uchida, T. Kikkawa, Z. Qiu, E. Saitoh, and K. Takanashi, *Observation of inverse spin Hall effect in ferromagnetic FePt alloys using spin Seebeck effect*, Appl. Phys. Lett. **107**, 092401 (2015).
[44] A. Tsukahara, Y. Ando, Y. Kitamura, H. Emoto, E. Shikoh, M. P. Delmo, T. Shinjo, and M. Shiraishi, *Self-induced inverse spin Hall effect in permalloy at room temperature*, Phys. Rev. B **89**, 235317 (2014).
[45] M. Wahler, N. Homonnay, T. Richter, A. Muller, C. Eisenschmidt, B. Fuhrmann, and G. Schmidt, *Inverse spin Hall effect in a complex ferromagnetic oxide heterostructure*, Sci. Rep. **6**, 28727 (2016).

[46] *H. L. Wang, C. H. Du, P. C. Hammel, and F. Y. Yang,* Spin current and inverse spin Hall effect in ferromagnetic metals probed by $Y_3Fe_5O_{12}$-based spin pumping*, Appl. Phys. Lett.* ***104****, 202405 (2014).*

[47] H. Wu, C. H. Wan, Z. H. Yuan, X. Zhang, J. Jiang, Q. T. Zhang, Z. C. Wen, and X. F. Han, *Observation of pure inverse spin Hall effect in ferromagnetic metals via ferromagnetic/antiferromagnetic exchange-bias structures*, Phys. Rev. B **92**, 054404 (2015).

[48] C. Qin, S. Chen, Y. Cai, F. Kandaz, and Y. Ji*, Nonlocal electrical detection of spin accumulation generated by anomalous Hall effect in mesoscopic* $Ni_{81}Fe_{19}$ *films,* Phys. Rev. B **96**, 134418 (2017).

[49] K. S. Das, W. Y. Schoemaker, B. J. van Wees, and I. J. Vera-Marun, *Spin injection and detection via the anomalous spin Hall effect of a ferromagnetic metal*, Phys. Rev. B **96**, 220408 (2017).

[50] D. C. Ralph and R. A. Buhrman, *Circuits and Devices Based on Spin Hall Effect to Apply a Spin Transfer Torque with a Component Perpendicular to the Plane of Magnetic Layers*, US Patent 9,691,458, submitted Oct. 20, 2014.

[51] T. Taniguchi, J. Grollier, and M. D. Stiles, *Spin-Transfer Torques Generated by the Anomalous Hall Effect and Anisotropic Magnetoresistance*, Phys. Rev. Appl. **3**, 044001 (2015).

[52] K. Garello, I. M. Miron, C. O. Avci, F. Freimuth, Y. Mokrousov, S. Blugel, S. Auffret, O. Boulle, G. Gaudin, and P. Gambardella, *Symmetry and magnitude of spin–orbit torques in ferromagnetic heterostructures*, Nat. Nanotechnol. **8**, 587 (2013).

[53] J. Kim, J. Sinha, M. Hayashi, M. Yamanouchi, S. Fukami, T. Suzuki, S. Mitani, and H. Ohno, *Layer thickness dependence of the current-induced effective field vector in Ta|CoFeB|MgO*, Nat. Mater. **12**, 240 (2013).

[54] C. O. Avci, K. Garello, M. Gabureac, A. Ghosh, A. Fuhrer, S. F. Alvarado, and P. Gambardella, *Interplay of S-O torque and thermoelectric effects in ferromagnet/normal-metal bilayers*, Phys. Rev. B **90**, 224427 (2014).

[55] M. Hayashi, J. Kim, M. Yamanouchi, and Hideo Ohno, *Quantitative characterization of the S-O torque using harmonic Hall voltage measurements*, Phys. Rev. B **89**, 144425 (2014).

[56] L. Liu, T. Moriyama, D. C. Ralph, and R. A. Buhrman, *Spin-Torque Ferromagnetic Resonance Induced by the Spin Hall Effect*, Phys. Rev. Lett. **106**, 036601 (2011).

[57] L. Liu, C. F. Pai, Y. Li, H. W. Tseng, D. C. Ralph, R. A. Buhrman, *Spin-Torque Switching with the Giant Spin Hall Effect of Tantalum,* Science **336**, 555 (2012).

[58] K. Ando, S. Takahashi, K. Harii, K. Sasage, J. Ieda, S. Maekawa, and E. Saitoh, *Electric Manipulation of Spin Relaxation Using the Spin Hall Effect*, Phys. Rev. Lett. **101**, 036601 (2008).
[59] K. Ando, Y. Kajiwara, S. Takahashi, S. Maekawa, K. Takemoto, M. Takatsu, and E. Saitoh, *Angular dependence of inverse spin–Hall effect induced by spin pumping investigated in a $Ni_{81}Fe_{19}$/Pt thin film*, Phys. Rev. B **78**, 014413 (2008).
[60] H. Y. Inoue, K. Harii, K. Ando, K. Sasage, and E. Saitoh, *Detection of pure inverse spin-Hall effect induced by spin pumping at various excitation*, J. Appl. Phys. **102**, 083915 (2007).
[61] X. Fan, A. R. Mellnik, W. Wang, N. Reynolds, T. Wang, H. Celik, V. O. Lorenz, D. C. Ralph, J. Q. Xiao, *All-Optical Vector Measurement of Spin-Orbit-Induced Torques Using Both Polar and Quadratic Magneto-Optic Kerr Effects*, Appl. Phys. Lett. **109**, 122406 (2016).
[62] Y. Fan, K. J. Smith, G. Lupke, A. T. Habicki, R. Goswami, C. H. Li, B. H. Zhao, and B. T. Jonker, *Exchange bias of the interface spin system at the Fe/MgO interface*. Nature Nanotech. **8**, 438 (2013).
[63] L. Berger, *Application of the Side-Jump Model to the Hall Effect and Nernst Effect in Ferromagnets*, Phys. Rev. B **5**, 1862 (1972).
[64] T. Miyasato, N. Abe, T. Fujii, A. Asamitsu, S. Onoda, Y. Onose, N. Nagaosa, and Y. Tokura, *Crossover Behavior of the Anomalous Hall Effect and Anomalous Nernst Effect in Itinerant Ferromagnets*, Phys. Rev. Lett. **99**, 086602 (2007).
[65] K. Uchida, H. Adachi, T. Ota, H. Nakayama, S. Maekawa, and E. Saitoh, *Observation of longitudinal spin-Seebeck effect in magnetic insulators*, Appl. Phys. Lett. **97**, 172505 (2010).
[66] S. Honda, M. Nawate, M. Ohkoshi, and T. Kusuda, *Hall Effect and Magnetic Properties in GdFe and CoCr Sputtered Films*, J. Appl. Phys. 57, 3204 (1985).
[67] N. Reynolds, P. Jadaun, J. T. Heron, C. L. Jermain, J. Gibbons, R. Collette, R. A. Buhrman, D. G. Schlom, and D. C. Ralph, *Spin Hall torques generated by rare-earth thin films*, Phys. Rev. B **95**, 064412 (2017).
[68] M. Ali, C. H. Marrows, M. Al-Jawad, B. J. Hickey, A. Misra, U. Nowak, and K. D. Usadel, *Antiferromagnetic layer thickness dependence of the IrMn/Co exchange-bias system*, Phys. Rev. B **68**, 214420.
[69] Y. Shen, Y. Wu, H. Xie, K. Li, J. Qiu, , and Z. Guo, *Exchange bias of patterned NiFe/IrMn film*, J. Appl. Phys. **91**, 8001 (2002).
[70] I. N. Krivorotov, N. C. Emley, J. C. Sankey, S. I. Kiselev, D. C. Ralph, R. A. Buhrman, *Time-Domain Measurements of Nanomagnet Dynamics Driven by Spin-Transfer Torques*, Science **307**, 228 (2005).

[71] M.-H. Nguyen, C.-F. Pai, K. X. Nguyen, D. A. Muller, D. C. Ralph, and R. A. Buhrman, "*Enhancement of the anti-damping spin torque efficacy of platinum by interface modification*,**"** Appl. Phys. Lett. **106**, 222402 (2015).
[72] Y. Ou, C.F. Pai, S. Shi, D. C. Ralph, and R. A. Buhrman, *Origin of fieldlike spin-orbit torques in heavy metal/ferromagnet/oxide thin film heterostructures*, Phys. Rev. B **94**, 140414(R) (2016).
[73] J. Liu, T. Ohkubo, S. Mitani, K. Hono, M. Hayashi, *Correlation between the spin Hall angle and the structural phases of early 5d transition metals,* Appl. Phys. Lett. **107**, 232408 (2015).
[74] R. Ramaswamy, X. Qiu, T. Dutta, S. D. Pollard, and H. Yang, *Hf thickness dependence of spin-orbit torques in Hf/CoFeB/MgO heterostructures*, Appl. Phys. Lett. **108**, 202406 (2016).

[75] M. Akyol, W. Jiang, G. Yu, Y. Fan, M. Gunes, A. Ekicibil, P. K. Amiri, and K. L. Wang, *Effect of heavy metal layer thickness on spin-orbit torque and current-induced switching in Hf|CoFeB|MgO structures*, Appl. Phys. Lett. **109**, 022403 (2016).
[76] C.-F. Pai, M.-H. Nguyen, C. Belvin, L. H. Vilela-Leão, D. C. Ralph, and R. A. Buhrman, *Enhancement of Perpendicular Magnetic Anisotropy and Transmission of Spin-Hall-Effect-Induced Spin Currents by a Hf Spacer Layer in W/Hf/CoFeB/MgO Layer Structures*, Appl. Phys. Lett. **104**, 082407 (2014).

[77] C.-F. Pai, M.-H. Nguyen, C. Belvin, L. H. Vilela-Leão, D. C. Ralph, and R. A. Buhrman, *Enhancement of Perpendicular Magnetic Anisotropy and Transmission of Spin-Hall-Effect-Induced Spin Currents by a Hf Spacer Layer in W/Hf/CoFeB/MgO Layer Structures*, Appl. Phys. Lett. **104**, 082407 (2014).

[78] A. M. Humphries, T. Wang, E. R. J. Edwards, S. R. Allen, J. M. Shaw, H. T. Nembach, J. Q. Xiao, T. J. Silva, and X. Fan, *Observation of Spin-Orbit Effects with Spin Rotation Symmetry*, arXiv:1704.08998 (2017).

[79] S. Iihama, T. Taniguchi, K. Yakushiji, A. Fukushima, Y. Shiota, S. Tsunegi, R. Hiramatsu, S. Yuasa, Y. Suzuki, and H. Kubota, *Spin-transfer torque induced by the spin anomalous Hall effect*, Nature Electronics **1**, 120 (2018).
[80] A. Mellnik. *Measurements of Spin Torques Generated by Topological Insulators and Heavy Metals*, PhD Thesis, Physics Department, Cornell University, 2015.
[81] M. Takahashi, T. Shimamori, T. Miyazaki, T. Wakiyama, and A. Yoshihara, IEEE Trans. J. Magn. Jpn. **4**, 666 (1989).
[82] J. Finley and L. Liu, *Spin-Orbit-Torque Efficiency in Compensated Ferrimagnetic Cobalt-Terbium Alloys*, Phys. Rev. Appl. **6**, 054001 (2016).